VOLUME 32 APRIL 1954 NUMBER 4

Canadian Journal of Physics

Editor: G. M. VOLKOFF

Associate Editors:

L. G. ELLIOTT, *Atomic Energy of Canada, Ltd., Chalk River*
J. S. FOSTER, *McGill University*
G. HERZBERG, *National Research Council of Canada*
L. LEPRINCE-RINGUET, *Ecole Polytechnique, Paris*
D. W. R. McKINLEY, *National Research Council of Canada*
B. W. SARGENT, *Queen's University*
F. E. SIMON, *Clarendon Laboratory, University of Oxford*
W. H. WATSON, *University of Toronto*

Published by THE NATIONAL RESEARCH COUNCIL
OTTAWA CANADA

CANADIAN JOURNAL OF PHYSICS

(*Formerly Section A, Canadian Journal of Research*)

The CANADIAN JOURNAL OF PHYSICS is published monthly by the National Research Council of Canada under the authority of the Chairman of the Committee of the Privy Council on Scientific and Industrial Research. The National Research Council publishes also: *Canadian Journal of Biochemistry and Physiology, Canadian Journal of Botany, Canadian Journal of Chemistry, Canadian Journal of Technology, Canadian Journal of Zoology.*

Matters of general policy concerning the Council's journals are the responsibility of a joint Editorial Board consisting of: the Editors of the journals; members representing the National Research Council of Canada and the Royal Society of Canada and three other scientific societies; and two ex-officio members.

EDITORIAL BOARD

Editors of the Journals

D. L. Bailey, *University of Toronto*
J. B. Collip, *University of Western Ontario*
E. H. Craigie, *University of Toronto*
G. A. Ledingham, *National Research Council*
Léo Marion, *National Research Council*
G. M. Volkoff, *University of British Columbia*

Representatives of the National Research Council

C. W. Argue (Chairman), *University of New Brunswick*
G. E. Hall, *University of Western Ontario*
T. Thorvaldson, *University of Saskatchewan*
W. H. Watson, *University of Toronto*

Representatives of Societies

D. L. Bailey, *University of Toronto*
Royal Society of Canada
J. B. Collip, *University of Western Ontario*
Canadian Physiological Society
E. H. Craigie, *University of Toronto*
Royal Society of Canada
H. G. Thode, *McMaster University*
Chemical Institute of Canada
T. Thorvaldson, *University of Saskatchewan*
Royal Society of Canada
G. M. Volkoff, *University of British Columbia*
Royal Society of Canada
Canadian Association of Physicists

Ex officio

Léo Marion (Editor-in-Chief)
National Research Council
H. H. Saunderson
National Research Council

Manuscripts should be addressed to:

Dr. Léo Marion,
Editor-in-Chief,
Canadian Journal of Physics,
National Research Council,
Ottawa 2, Canada.

Subscriptions, renewals, and orders for back numbers should be addressed to:

Division of Administration,
National Research Council,
Ottawa 2, Canada.

Subscription rate: $4.00 a year, single numbers: 75 cents. Remittances should be made payable to the Receiver General of Canada, credit National Research Council.

Canadian Journal of Physics

Issued by THE NATIONAL RESEARCH COUNCIL OF CANADA

VOLUME 32 APRIL 1954 NUMBER 4

AN IONIZATION MANOMETER AND CONTROL UNIT FOR EXTREMELY LOW PRESSURES[1]

BY P. A. REDHEAD AND L. R. MCNARRY

ABSTRACT

A Bayard-Alpert type ionization manometer for the measurement of pressures as low as 10^{-10} mm. of mercury is described, and methods for increasing the sensitivity are discussed. The control unit is direct reading in pressure to 10^{-10} mm. and has provision for degassing the electrodes.

1. INTRODUCTION

Conventional ionization manometers have a lower limit to the pressure they can measure which occurs when photoemission from the ion collector is of the same magnitude as the positive ion current to the collector. The photoemission from the ion collector is caused by soft X-rays produced by electron bombardment of the positive grid. This lower limit is about $10^{-6} - 10^{-7}$ mm. in most conventional manometers. In order to measure lower pressures it is necessary to decrease the X-ray induced photoemission; this may be achieved by shielding the ion collector from the X-radiation or by reducing the surface area of the ion collector. The first method has been suggested by Lander (3) and Metson (4). The second method, in which the ion collector is exposed to the X-radiation but the surface area of the collector is reduced, lends itself to a simple design with high ion trapping efficiency. This type of design was first proposed by Bayard and Alpert (1, 2); the manometer herein described is of this type.

2. DESCRIPTION AND PERFORMANCE OF MANOMETER

The manometer tube has a double filament (see Fig. 1) of pure tungsten outside the electron collecting grid (molybdenum). At the center of the electron grid is the positive ion collector consisting of a fine tungsten wire. The electrodes are enclosed in a spherical bulb to reduce the danger of the envelope overheating when the electrodes are outgassed.

The relevant dimensions are:—

Filament—0.010 in. diam. tungsten wire spirals, total length of wire 1.5 in. Filament supports 0.040 in. diam. molybdenum. A tensioning spring prevents sagging of the filament.

[1] *Manuscript received November 18, 1953.*
Contribution from the Radio and Electrical Engineering Division, National Research Council, Ottawa, Canada. Issued as N.R.C. No. 3217.

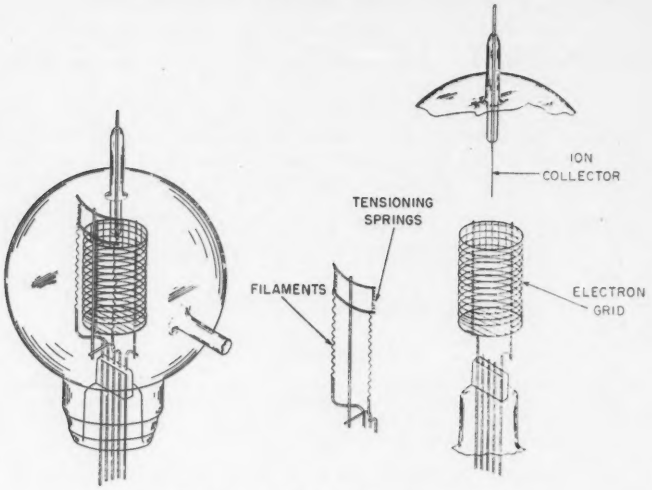

FIG. 1. Drawing of manometer.

Electron grid—1.0 in. diam. and 1.5 in. long. The grid is of 0.005 in. diam. molybdenum wire wound 10 T.P.I. on four 0.029 in. diam. molybdenum supports. The ends of the grid are enclosed by six 0.005 in. diam. molybdenum wires.

Ion collector—0.003 in. diam. tungsten wire extending 1.4 in. into the grid cage. The lead outside the grid cage is shielded by a glass tube.

Bulb—Pyrex glass.

It is worth noting that the tube contains no materials other than tungsten or molybdenum thus allowing the electrodes to be outgassed at high temperatures without damage.

The operating characteristics of the manometer are shown in Figs. 2, 3, and 4. Fig. 2 shows the ion collector characteristic, the sensitivity factor of the manometer (K) being given by

$$K = \frac{i_+}{i_-} \cdot \frac{1}{p} \text{ (mm.}^{-1}\text{)}$$

where i_+ and i_- are the positive ion and electron currents, respectively, and p is the pressure in millimeters. It will be seen that the sensitivity is effectively constant provided that the collector potential is less than -25 v.

The slight upward slope of this characteristic shows that the collector is not behaving as a perfect ion trap. As the collector is made more negative the ionizing volume is reduced and a slight downward slope would be expected if the collector were trapping all the ions.

Fig. 3 shows the variation of sensitivity with the potential of the electron grid for dry nitrogen. Maximum sensitivity occurs when the electron grid potential is about $+90$ v.

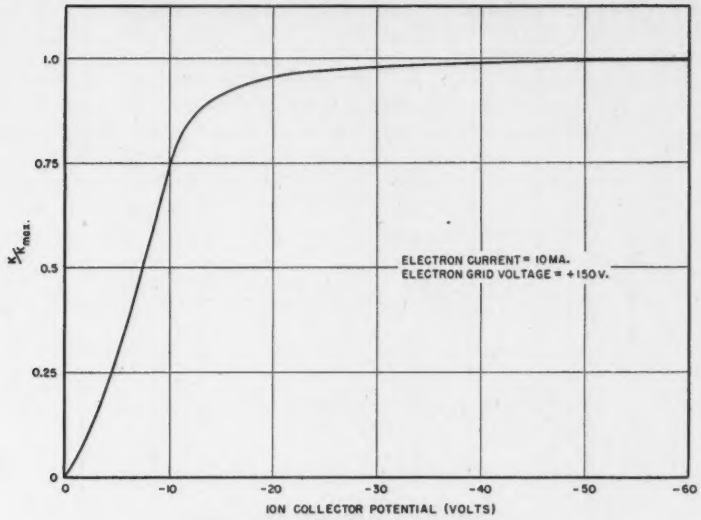

FIG. 2. Ion collector characteristic.

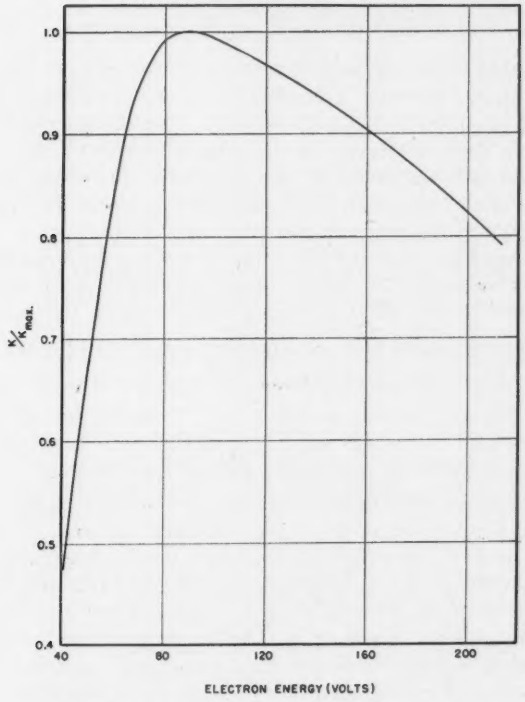

FIG. 3. Variation of sensitivity with electron energy.

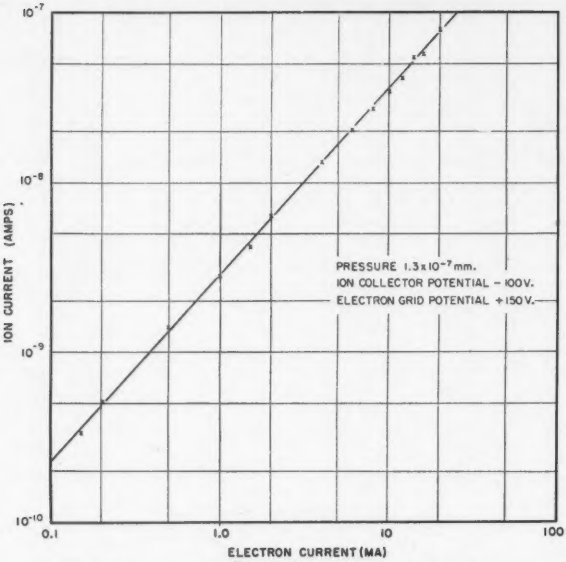

FIG. 4. Ion current vs. electron current characteristic.

Fig. 4 shows the linear relationship between electron current and ion current. At high ion currents the ionic space-charge in the grid–collector region causes a deviation from linearity. The ion current at which space-charge becomes appreciable has been calculated for the above dimensions, for a potential of 150 v. between grid and collector, and was found to be approximately one microampere for nitrogen ions. This critical current sets the upper limit of pressure which may be measured with this manometer.

The photoemission from the ion collector due to the light from the hot filaments was measured and found to be sufficiently small that no errors would be caused by this effect at pressures above about 10^{-14} mm.

3. METHODS FOR INCREASING THE SENSITIVITY

The sensitivity of this type of manometer may be increased by:—

(1) Increasing the ionizing volume (i.e., increasing the diameter of the electron grid).

(2) Improving the ion trapping efficiency of the collector.

(3) Increasing the path length of an electron in the ionizing region before it is captured by the electron grid, thus increasing the ionization probability.

The electron grid diameter of 1 in. seems to be a reasonable compromise between sensitivity and size. A larger grid makes the tube difficult to outgas.

Closing the ends of the grid cylinder improves the ion trapping at the collector. The collector length affects the trapping efficiency most markedly. In the first tubes the collector wire was too short and the collector characteristic did not saturate; extending the collector produced satisfactory ion trapping.

The path length of the electrons before capture at the electron grid may be increased by placing a shield grid outside the filament and electron grid. When this grid is negative the focusing of the electrons through the wires of the electron grid is improved and their effective path length before capture at the grid increased. Fig. 5 shows the change in sensitivity as the potential

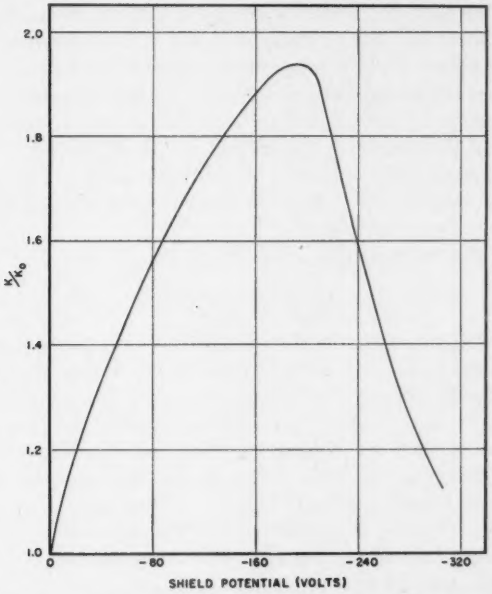

FIG. 5. Variation of sensitivity with external shield potential.

of the shield grid is varied. The shield grid was 1.75 in. diam. of 0.005 in. molybdenum wire wound 10 T.P.I. on 0.030 in. diam. molybdenum supports. This shield also prevents electron bombardment of the glass and thus fixes the potential of the surface of the glass bulb. It was found that this grid completely prevented the pumping action which is normally observed in ionization manometers.

The shield grid was not used in the final design since it is difficult to outgas thoroughly by electron bombardment and because it prevents the use of the tube as an ionization pump. In cases where very high sensitivities are desired the shield grid should be employed.

Typical operating conditions are:—

Filament voltage (approx.)	12.5 v.
Filament current (approx.)	5 amp.
Electron current	10 ma.
Maximum ion current	1 μa.
Sensitivity (K)	26 mm.$^{-1}$

4. MANOMETER CONTROL CIRCUIT

Regulation of the electron current of the ionization manometer is obtained by means of a variable impedance reflected into the filament circuit of the tube. A type 2D21 thyratron, V_5, (see the complete circuit diagram shown in Fig. 6) was chosen as the variable impedance element. It has an intrinsically high gain and its effective impedance may be varied over wide limits. The magnitude of the electron current is set by the potentiometer P_1. Any changes in grid potential of V_{4a} due to changes in the electron current are amplified by the d-c. amplifier V_{4a} which in turn controls the grid of V_5. The value of the electron current is measured in terms of the voltage drop across P_1 when S_5 is in position 2. To prevent low frequency oscillations, due to the thermal time-constant of the manometer tube filament, it is necessary to place a 10μf. capacitor across the 68K resistor in the cathode circuit of V_5. The collector potential of approximately -50 v. is obtained from the voltage drop across the 3.9K resistor in series with P_1.

The electron current may be varied from 2.5 to 25 ma.

4a. ELECTROMETER

The balanced electrometer used to measure the ion current uses two Victoreen type 5800 tubes which are operated from a 9 v. dry battery. The range switch S_7, the grid resistors, the bias resistors, and the two tubes are enclosed in a hermetically sealed metal case with a capsule containing a desiccant attached. The stability of cathode emission of the electrometer tubes is improved by delaying the application of the $B+$ voltage relative to the application of the filament voltage. The $B+$ voltage is also removed before the filament voltage. This is accomplished by two relays RY-1 and RY-2 which are operated from the 150 v. $B+$ line; RY-1 controls the $B+$ voltage to the electrometer tubes and RY-2 the filament voltage.

The R-C time constants in the relay circuit are chosen to delay the closure of RY-1 with respect to RY-2 on applying the 150 v. $B+$ and to delay the opening of RY-2 with respect to RY-1 on removing the 150 v. supply. The delay in each case is about one second.

The battery voltage is read with S_5 in position 1 and the zero and sensitivity of the electrometer are adjusted with S_5 in position 3.

The control unit may be made direct reading in pressure by proper choice of the electron current and setting of the electrometer sensitivity control (P_2).

5. OUTGASSING

In order to provide adequate emission for electron bombardment of the grid and collector the temperature of the filament is raised from 1760°C., where it normally operates, to a temperature sufficient to provide about 200 ma. for a grid potential of 700 v. r.m.s. Either the grid alone or both grid and collector may be bombarded. For degassing, the contacts of relay RY-3 short circuit the control transformer and ground the center tap of the filament to isolate the control circuit, and also insert an additional 10 v. filament transformer

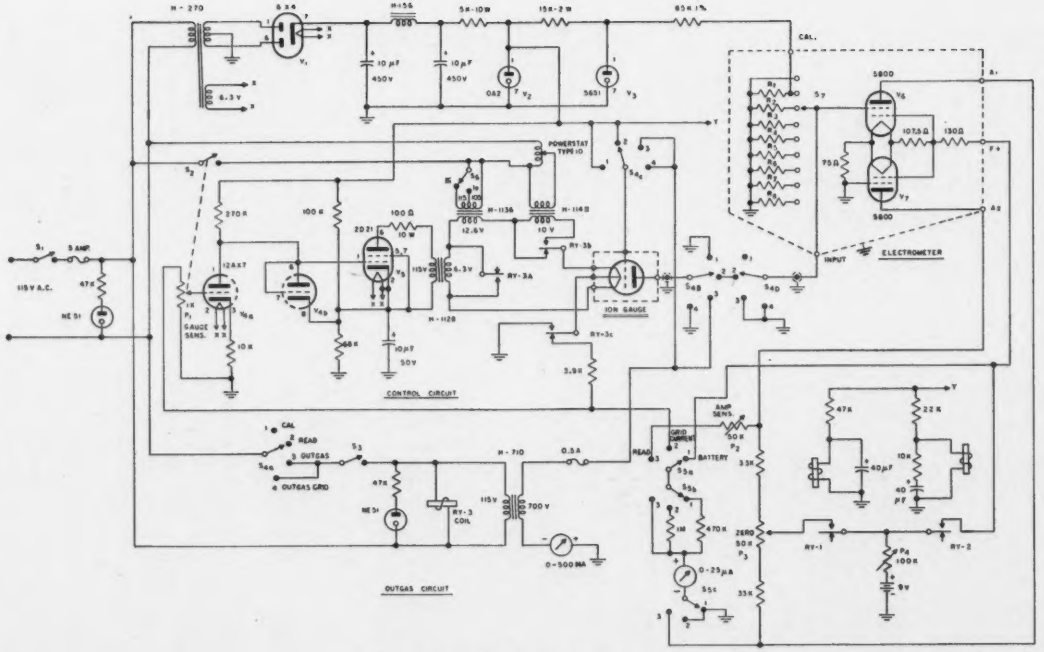

RESISTORS
R_1—1 K, 1%.
R_2—100 K.
R_3—1 meg.
R_4—10 meg.
R_5—100 meg.
R_6—1000 meg.
R_7—10,000 meg.
R_8—100,000 meg.

FIG. 6. Schematic circuit diagram.

NOTES:

All resistors ½ watt unless otherwise specified.
S_4—four-gang four-position low-loss switch insulated for 1500 v. (Centralab 2545).
RY-3—contacts must carry up to 10 amp.
S_3—microswitch operated by powerstat.
P_4—adjusted so that current at $F+$ is 20 ma. Mark this reading on meter face when S_8 in position 1.
S_2—ganged with P_1 (gauge sensitivity).
S_6—mounted on chassis.
RY-1, 2—Potter and Brumfield relay type SM5LS—10,000Ω.

into the filament circuit. The switching in the degas circuit is interlocked so that all circuits are protected during the degassing process.

REFERENCES

1. ALPERT, D. J. Appl. Phys. 24: 860. 1953.
2. BAYARD, R. T. and ALPERT, D. Rev. Sci. Instr. 21: 571. 1950.
3. LANDER, J. J. Rev. Sci. Instr. 21: 672. 1950.
4. METSON, G. H. Brit. J. Appl. Phys. 2: 46. 1951.

FAST NEGATIVE HYDROGEN IONS[1]

By A. Charles Whittier[2]

ABSTRACT

A proton beam was directed through hydrogen gas at low pressure and magnetic analysis of the emergent beam showed that an appreciable fraction of the beam was transformed into negative hydrogen ions. After the beam had traversed a sufficient layer of gas, the ratio of negative hydrogen ions to protons reached an equilibrium value which was a maximum of 22.2% at 8.5 kev. The proton energy interval investigated extended from 4 to 70 kev.

In this interval the electron loss cross section for negative hydrogen ions was measured and found to vary from 6.3×10^{-16} sq. cm. at 4.2 kev. to 2.5×10^{-16} sq. cm. at 70.3 kev. The electron capture cross section for protons in hydrogen was measured over the same interval and the results agreed substantially with those of other workers. The electron capture cross section for neutral atoms was also determined by combining present results for the negative ion loss cross section and for the equilibrium ratio of H^- to H^+ with the values of Bartels and of Montague and Ribe for the ratio of neutral atom loss cross section to the proton capture cross section.

INTRODUCTION

When a beam of accelerated protons passes through a gas, some of the protons capture an electron and become neutral atoms. Some of the latter capture a further electron and become negative hydrogen ions. The purpose of the present work was to study this process in hydrogen gas and primarily to determine the electron loss cross section for negative hydrogen ions in the energy interval from 4 to 70 kev. The cross sections for other associated phenomena were also found.

The formation of negative hydrogen ions under various conditions was reported by Tuxen (16), Arnot (1), Lofgren (9), and Ribe (14). Hasted (4) determined the electron loss cross section for H^- passing through the noble gases in the energy region from 100 to 3000 ev. A number of experiments, using a variety of methods (2, 3, 7, 14), have been performed to determine the electron capture cross section for protons. Since the results of these are not completely consistent, this cross section has also been determined in the present work.

METHOD

The method used in the present work is illustrated in diagrammatic form in Fig. 1.

A beam of protons emerges from the lower end of an accelerating tube and enters a field-free ion exchange chamber containing hydrogen through aperture (A). Some of these protons will capture electrons in this space and become neutral hydrogen atoms. Of the latter, some will lose their electrons to become protons again, and others will capture a further electron to become negative

[1] *Manuscript received November 20, 1953.*
Contribution from the Radiation Laboratory, McGill University, Montreal. Based on a Ph.D. thesis.

[2] *Holder of a Research Council of Ontario Scholarship 1950-51, and a National Research Council Studentship 1951–52. Now with Atomic Energy of Canada Limited, Chalk River, Ontario.*

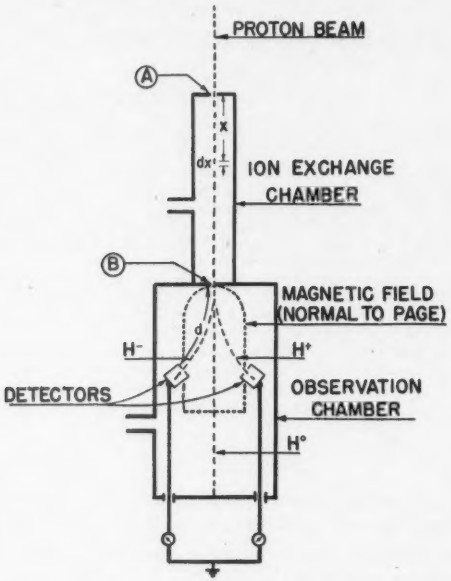

FIG. 1. Protons passing through hydrogen gas in the ion exchange chamber capture electrons to form H^0 and H^-. The resultant mixed beam is analyzed in the observation chamber.

hydrogen ions. The process taking place in the "ion exchange chamber" can be treated as follows.

Let I be the incident proton current at (A). Let H^+, H^-, and H^0 represent the currents of protons, negative hydrogen ions, and neutral atoms respectively, in the beam at a distance x from aperture (A).

Assuming the formation of negative hydrogen ions by protons capturing two electrons simultaneously to be relatively improbable, the relevant differential equations are:

$$[1] \qquad dH^+ = H^0 n\sigma_l{}^0\, dx - H^+ n\sigma_c{}^+\, dx,$$

$$[2] \qquad dH^- = H^0 n\sigma_c{}^0\, dx - H^- n\sigma_l{}^-\, dx,$$

$$[3] \qquad I = H^+ + H^- + H^0,$$

where $\sigma_c{}^+$ is the electron capture cross section for a proton,
$\sigma_c{}^0$ is the electron capture cross section for a neutral atom,
$\sigma_l{}^0$ is the electron loss cross section for a neutral atom,
$\sigma_l{}^-$ is the electron loss cross section for a negative H ion, and
n is the number of gas atoms per cc. in the ion exchange chamber.

After sufficient gas has been traversed by the beam its components will reach equilibrium with one another and the following relation will apply:

$$[4] \qquad (H^-/H^+)_e = (\sigma_c{}^0/\sigma_l{}^-)(\sigma_c{}^+/\sigma_l{}^0).$$

The subscript e refers to the ratio under equilibrium conditions.

The beam of particles, whose components have already reached equilibrium, emerges through aperture (B) into the "observation chamber" where the particles are subjected to a magnetic field at right angles to their direction of motion. The components of the beam will be separated by the magnetic field and the positive and negative ions will describe paths of opposite curvature ending in the detectors, as shown.

The observation chamber also contains hydrogen gas whose pressure can be varied.

Interactions between ions and gas molecules will also take place in this chamber. Thus a negative ion may lose an electron, leave its curved path, and fail to enter the detector. Similarly, a positive ion on capturing an electron will also leave its curved path and fail to enter the detector. Bearing in mind that the curved beam into either detector consists exclusively of ions of one kind and that any interaction can only lead to losses in this beam, it is easy to show that

$$H^+ = H_e^+ e^{-kp_0\sigma_c^+ d}, \tag{5}$$

$$H^- = H_e^+ e^{-kp_0\sigma_i^- d}, \tag{6}$$

where H^+ and H^- are the number of protons and negative ions reaching their respective detectors and the subscript e refers to the equilibrium values of these numbers as the ions emerge from aperture (B). $k = 1.93 \times 10^{19}/T_{abs}$; p_0 is the pressure of hydrogen in the observation chamber in mm. of Hg, and d is the length of curved path from aperture (B) to either detector.

APPARATUS

The Ion Accelerator (17)

Positive ions were produced in a pyrex capillary arc type of ion source (8) and accelerated in an apparatus of the Cockcroft-Walton type. D-c. power for the ion source was supplied by a motor generator set (with a bakelite shaft coupling) mounted on an insulating table. The ions were focused and accelerated by a series of cylindrical dural electrodes. Accelerating potentials were obtained from a seven-stage r-f. high voltage multiplier circuit operating at 102 kc.

A novel feature of the circuit was an r-f. supply for the filaments of the fourteen 8016 rectifiers of the voltage multiplier. A series of r-f. isolating transformers and tuning condensers formed the plate tank circuit of an independent 1300 kc. oscillator. The diode filaments were inductively coupled to the transformers by wire loops.

D-c. output voltages were measured with a carefully calibrated galvanometer and high resistance, and the ripple voltage did not exceed 0.2%.

Ion Exchange Chamber

The ion exchange chamber is shown in the upper half of Fig. 2. The ion beam from the accelerator entered this chamber through the isolating capillary whose internal diameter was 1 mm. The isolating capillary was so mounted that it could be accurately aligned to allow the focused beam of ions to pass through it. In order to facilitate this adjustment, an insulated probe passing

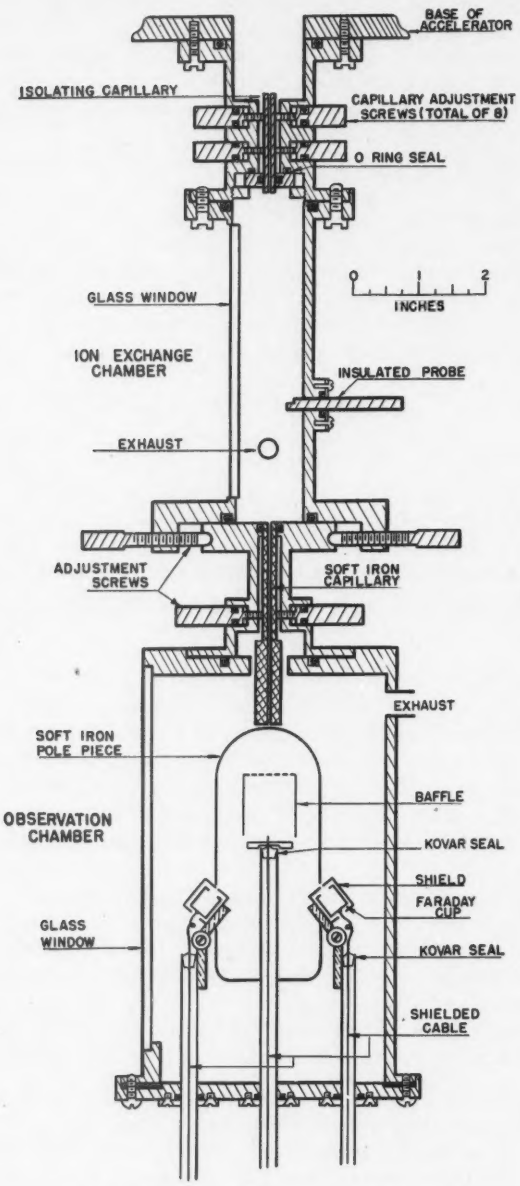

FIG. 2. Diagram of the experimental chambers.

through an O-ring seal in the side of the chamber could be moved into the path of the beam and the collected current measured. A glass observation window formed one side of the exchange chamber.

The pressure, p_i, of hydrogen in this chamber was controlled by an independent pumping system and could be adjusted from 2×10^{-4} mm. Hg to 0.25 mm. Hg without affecting the operation of the accelerator tube.

Observation Chamber

The ion beam emerged from the ion exchange chamber through the soft iron isolating capillary shown, into the observation chamber where the components of the beam were resolved by a transverse magnetic field. In order to obtain a fixed magnetic field, pole pieces of soft iron were embedded in the brass side walls of the observation chamber, with a gap of ½ in. between the pole faces. Two pairs of magnetron permanent magnets mounted in contact with the outer faces of the pole pieces provided a steady field of about 2400 gauss.

The ion detectors for the positive and negative ions consisted of carefully shielded Faraday cups. The latter were mounted adjustably on the ends of brass tubes which could slide vertically through O-ring seals in the base of the chamber. Ions could only enter the detectors after passing through defining slits of 1.7 mm. width in the detector shields. These entrance slits, and indeed the entire detectors, were situated in such a magnetic field that secondary electron emission could not affect the current measurements.

Coaxial with the central axis of the original proton beam and of the isolating capillaries, was a third collecting electrode, mounted on a vertical brass tube passing through an O-ring seal in the base. This central electrode was in the form of a flat rectangular metal box, open at the top and provided with slits 2 mm. wide at its lower opposite edges as shown. Thus this assembly served not only as a beam collector but as a baffle to eliminate undesired secondary effects. This will be discussed further.

Gas pressure in the observation chamber was controlled by an adjustable hydrogen leak, a liquid air trap, and an oil diffusion pump and was measured by an ionization gauge. The pressure in this chamber could be varied between 3×10^{-5} and 1.2×10^{-2} mm. of Hg.

The isolating capillary connecting the two chambers had an inside diameter of 1 mm. and was made of soft iron in order to shield completely the ion beam from the magnetic field until it entered the observation chamber. The mountings of this capillary and of the flange attaching the observation to the ion exchange chamber were so designed that it was easy to align the capillary to coincide with the axis of the accelerated ion beam. At the same time the center line of the magnetic field coincided with this axis and the entrance slits of the ion detectors were equidistant from the center line. Thus ions entered the observation chamber along its center line, and those of opposite sign but equal energy described exactly similar curved paths to the entrance slits of their respective detectors. Since the magnetic field was constant, and the geometry was accurately known, it was possible to determine the path

length, d, (cf. Fig. 1) and the energy for an ion of given charge and mass reaching either detector, in terms of the vertical setting of the tube supporting that detector. Careful experiment showed that the path lengths for ions which differed in sign but in no other respect agreed within 2% even for ions of the lowest energy.

Ion Current Measurement

Positive and negative ion currents to the detectors, and their ratio, were measured by means of a ratio resistance circuit in conjunction with an FP-54 electrometer tube and galvanometer. The arrangement is shown in Fig. 3

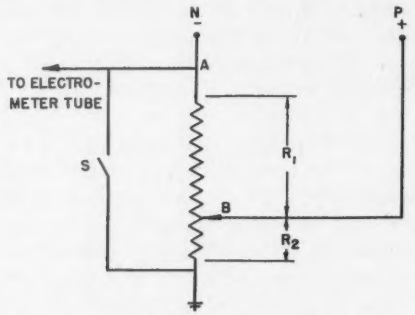

FIG. 3. The ratio resistance circuit for measuring negative and positive ion currents and their ratio.

where shielded leads from the positive and negative ion detectors connect to points P and N respectively. The voltage developed at A was applied directly to the electrometer tube grid and the maximum value of $R_1 + R_2$ was 130 megohms. The negative ion current i^- could be measured when the sliding contact B was grounded. The ratio $(i^-/i^+) = R_2/(R_1 + R_2)$ was obtained by adjusting B until the voltage at A was zero. The grounding switch, S, allowed frequent checks of the null point to be made.

EXPERIMENTAL PROCEDURE

Alignment of Chambers and Capillaries

A parallel beam of ions usually 1 to 1.5 mm. in diameter was first obtained in the ion accelerator. The insulated probe in the ion exchange chamber (Fig. 2) was moved into position so that it collected any ions passing through the first capillary. This capillary was aligned until a maximum current was detected by the probe which was then withdrawn from the path of the beam. The central collecting electrode ("baffle") of the observation chamber was moved up close to the lower isolating capillary, and both the position of the observation chamber itself and the direction of the soft iron capillary were adjusted until the ion current to the electrode was a maximum. The central electrode was then lowered to the bottom of the chamber.

Beam Analysis

With both ion exchange and observation chambers evacuated to their minimum pressure and the accelerating potential maintained at 12.6 kv., an analysis of the ion beam entering the observation chamber was made. The positive ion detector was displaced vertically, in steps of 1 mm., and the positive ion current measured at each point. The results are shown in Fig. 4 where the abscissae refer to the vertical setting of the detector. Fig. 5 shows

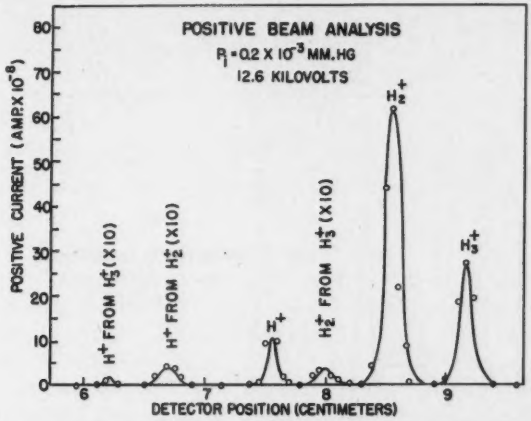

FIG. 4. Analysis of the accelerator beam at 12.6 kev. Some of the molecular ions H_2^+ and H_3^+ were dissociated when they encountered molecules of the residual gas in the base of the accelerator and in the ion exchange chamber; molecular and atomic ions resulting from this dissociation were collected at 8, 6.7, and 6.2 cm. (The "detector positions" indicated are merely distances measured from an arbitrary reference point to an indicator on the tubular detector mounting.)

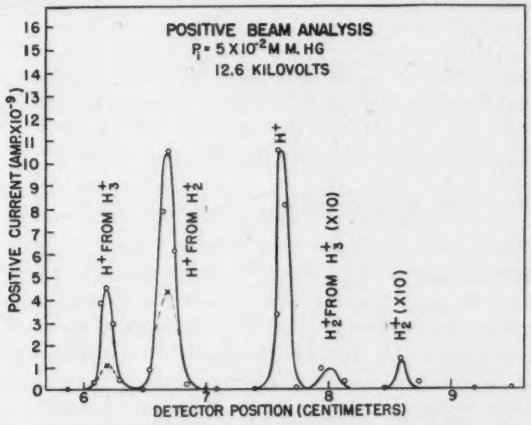

FIG. 5. Analysis of the positive components of the beam which had passed through hydrogen gas in the ion exchange chamber where the pressure was 5×10^{-2} mm. Hg. The heights of the peaks observed when the ion exchange chamber was evacuated are shown by "×"'s.

the results obtained for the positive ions when the ion exchange chamber pressure was raised to 5×10^{-2} mm. of Hg. In Fig. 4 the two peaks at the extreme right correspond to molecular ions H_3^+ and H_2^+; the peak at 8 cm. corresponds to H_2^+ ions arising from the partial dissociation of H_3^+. The peak at 7.6 cm. is due to protons accelerated through the full 12.6 kv. The peaks at 6.7 and 6.2 cm. are due to protons arising from the dissociation of molecular ions of H_2^+ and of H_3^+ respectively. That this dissociation takes place mostly in the ion exchange chamber can be seen from a comparison of the two curves.

A similar analysis was carried out for the negative ions in the beam, with results of which Fig. 6 is typical. Only three peaks were obtained under all

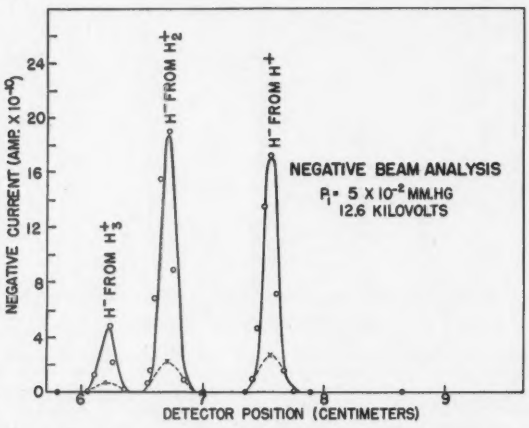

FIG. 6. Analysis of the negative ion components of the beam which entered the observation chamber. The heights of the peaks when the ion exchange chamber was evacuated are indicated by ×'s.

conditions, and no evidence at all was found for negative ions of mass greater than one. The left-hand peaks represent negative ions formed from H_2^+ and H_3^+ respectively. At very low pressures in the ion exchange chamber, the negative ion peaks shrank to the proportions shown by the crosses on the dotted lines.

Note that the ordinate scales differ in Figs. 4, 5, and 6.

Equilibrium Ratio

The equilibrium ratio of negative to positive ions in the beam was studied by evacuating both chambers to as low pressures as possible and placing the detectors so that they collected protons and negative ions whose energies corresponded to that of the protons accelerated by the full potential drop of the accelerator. The disposition may be seen in Fig. 7. Under these conditions the negative ion current, i^-, the ratio (i^-/i^+), the pressures p_i and p_0 were recorded. The pressure p_i was increased in steps to about 0.16 mm. of Hg, and the above four readings were recorded at each step. Leakage of gas

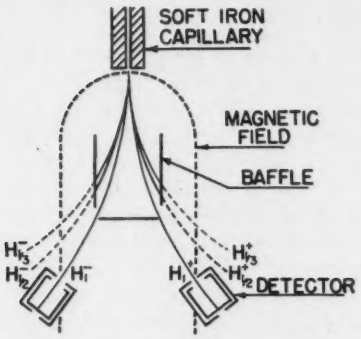

FIG. 7. The positions of the beam components in the observation chamber after the beam had reached equilibrium in the ion exchange chamber. The baffle effectively blocked the undesired beam components from affecting the cross-section measurements by multiple charge exchange.

through the soft iron capillary led to a slight increase of pressure p_0 in the observation chamber as p_i was increased. As a result some charge exchange took place between the resolved components of the beam and gas molecules in the observation chamber. The values of both i^- and of (i^-/i^+) were corrected for this effect. The ratio (i^-/i^+) or (H^-/H^+) increased as the pressure in the ion exchange chamber was raised until it reached an equilibrium value $(H^-/H^+)_e$ at a pressure p_i which in all cases was less than 5×10^{-2} mm. of Hg. At all pressures above this, the equilibrium ratio remained constant for a given accelerating voltage.

The value of the equilibrium ratio was found to be the same whether the ions came from the original proton beam or from the dissociation of molecules in the ion exchange chamber. Thus $(H^-/H^+)_e$ was obtained with a 12 kev. proton beam; with the protons arising from the dissociation of an H_2^+ beam which had been accelerated through 24 kv.; and with protons arising from the dissociation of an H_3^+ beam accelerated through 36 kv. In all cases the values obtained for $(H^-/H^+)_e$ were identical within the limits of error of the measurements.

The effect of scattering was studied by applying the formula for multiple scattering (12) to interactions between atomic ions in the beam and gas molecules in the ion exchange chamber. This effect was found quantitatively to account for the observed reduction in the number of ions of either sign received by the detectors as p_i was increased to high values. The ratio $(H^-/H^+)_e$ was not affected by scattering.

Applying the same scattering formula to the conditions prevailing in the observation chamber, it was concluded that the effects of scattering in this region were negligible. This was tested experimentally and it was found that over the whole range of pressures employed in the observation chamber no broadening of the ion beam could be detected. This was consistent with the observations of Ribe (14).

Multiple Charge Exchange

Fig. 7 shows the relative paths of the positive and negative components of the ion beam in the observation chamber. In this figure, the setting of the ion detectors is such that they are collecting atomic ions arising from the original proton beam. The curved paths bearing the subscripts $\frac{1}{2}$ and $\frac{1}{3}$ refer to atomic ions of either sign, arising from molecular ions of mass two and of mass three respectively, which arose in the ion source and were accelerated through the full potential drop of the accelerator tube.

It is evident that as the pressure p_0 in the observation chamber is raised, multiple charge exchange may take place between the ions entering the observation chamber and gas molecules in the latter. Thus a $H_{\frac{1}{2}}^+$ ion might capture an electron and leaving its curved path tangentially might become re-ionized and find its way to the detector. This would lead to more ions being detected at higher pressures than one would expect.

In order to prevent this, a rectangular baffle was attached to the central detector as shown in Fig. 2. Symmetrically placed slits at the opposite bottom corners of the baffle system allowed only the desired ions to reach the detectors.

One might expect that multiple charge exchange would take place within the ion beams actually being detected. This process was studied rather carefully by Kanner (6) and a consideration of his findings shows that the effect in the present experiment was negligible.

Formation of Negative Ions

Careful tests were made to establish that the negative hydrogen ions were formed by the interaction of the protons with gas molecules and not by interaction with the walls of the capillaries. Thus at low pressures the ratio (H^-/H^+) was measured with the capillaries in place and with no capillaries at all. In spite of the low pressures enough gas molecules were present to give rise to negative ions and the ratio (H^-/H^+) was exactly the same whether the capillaries were in place or were removed. On the other hand, any change in the nature of the gas in the ion exchange chamber gave rise to marked changes in the (H^-/H^+) ratio. Thus in air the ratio was one third of its value in hydrogen under the same conditions.

It was also found that slight lateral displacement or change in alignment of the iron capillary had no effect on the (H^-/H^+) ratio. This showed not only that the iron capillary provided effective magnetic shielding of the ion beam passing through it, but that protons striking the walls of the capillary did not thereby give rise to negative ions. Substitution of a brass capillary for the iron capillary used exhibited all the effects which would be expected from lack of magnetic shielding in the capillary region.

Energy Loss in the Gas

An attempt was made to determine the loss of energy suffered by the protons in passing through the gas column (length 12.5 cm.) in the ion exchange chamber. Both chambers were evacuated to the lowest possible pressure and the positive ion detector adjusted to collect the proton beam. The pressure p_i in the ion exchange chamber was then raised to 6×10^{-2} mm. of Hg and the

ion detector adjusted to detect any resulting shift in the proton beam. An energy change of less than 3% could have been detected. Even at the lowest energy used, viz. 4.2 kev., no shift could be detected. This upper limit of 3% for the energy loss is consistent with the results of Phillips (13) down to 10 kev., and with a reasonable extrapolation of his results down to 4 kev.

RESULTS

In order to determine the equilibrium ratio $(H^-/H^+)_e$ corresponding to a given energy of the accelerated protons, the procedure already described was followed. The pressure of hydrogen in the ion exchange chamber was maintained between 5 and 6 $\times$ 10^{-2} mm. of Hg. The ion detectors and the central baffle system were adjusted as shown in Fig. 7. The observation chamber pressure, p_0, was increased in steps of about 10^{-3} mm. of Hg, and the corresponding readings of (i^-/i^+), i^-, and of p_0 recorded at each step. When p_0 reached a value of 1.2 $\times$ 10^{-2} mm. of Hg the pressure was reduced in steps and the same readings repeated. This procedure was repeated several times at each energy and the ion detector settings and temperature noted.

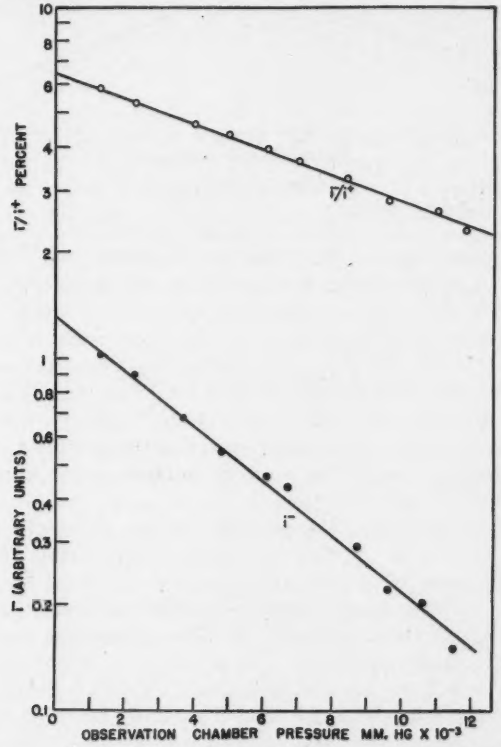

FIG. 8. One of six pairs of experimental curves of log i^- and log (i^-/i^+) versus observation chamber pressure p_0 at 25.6 kev.

A semilog plot of (i^-/i^+) against p_0 was drawn for each set of readings and the resulting straight lines produced to intercept the ordinate axis. This intercept gave the equilibrium ratio $(H^-/H^+)_e$ corresponding to zero pressure in the observation chamber. A typical example of one of six such curves obtained at 25.6 kev. is shown in Fig. 8. Thus for a given energy the value of $(H^-/H^+)_e$ obtained is the average taken from the intercepts of from four to six similar curves.

The values of the equilibrium ratio finally obtained are given in Fig. 9 and in Table I over the range from 4 to 70 kev.

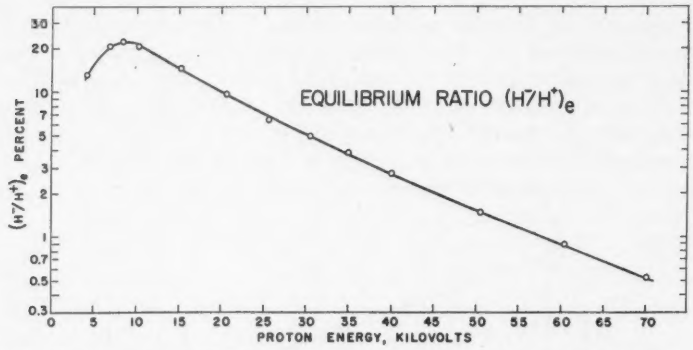

FIG. 9. The variation of $(H^-/H^+)_e$ with energy of protons incident on the hydrogen gas in the ion exchange chamber.

Log i^- was plotted against p_0 for each set of readings and a typical curve is shown in Fig. 8. In every case, a straight line was obtained, as predicted in equation [6]. The slopes of the lines obtained in several sets of readings were averaged, and since the slope is equal to $-kd\sigma_l^-$, division by the appropriate value of kd yields a value of σ_l^-, the electron loss cross section for negative ions. The values obtained for the electron loss cross section over the whole energy range are given in Table I and plotted against energy in Fig. 10.

Throughout this work, the minimum stable accelerating voltage obtainable was 12.6 kv. and for energies less than this, protons arising from the dissociation of H_2^+ or of H_3^+ ions were used.

From the above results it is also possible to obtain values of σ_c^+, the electron capture cross section for protons. A consideration of equations [5] and [6] shows that the slope of the log (i^-/i^+) against p_0 curve will be equal to $kd(\sigma_c^+ - \sigma_l^-)$. If for a given energy, one subtracts from this the slope of the corresponding i^- versus p_0 curve, the difference of these slopes, divided by kd, will give the value of σ_c^+.

The values of σ_c^+ so obtained are given in Table I and in Fig. 10. For purposes of comparison with the values obtained by other workers, these results are also given in the curve marked A in Fig. 11.

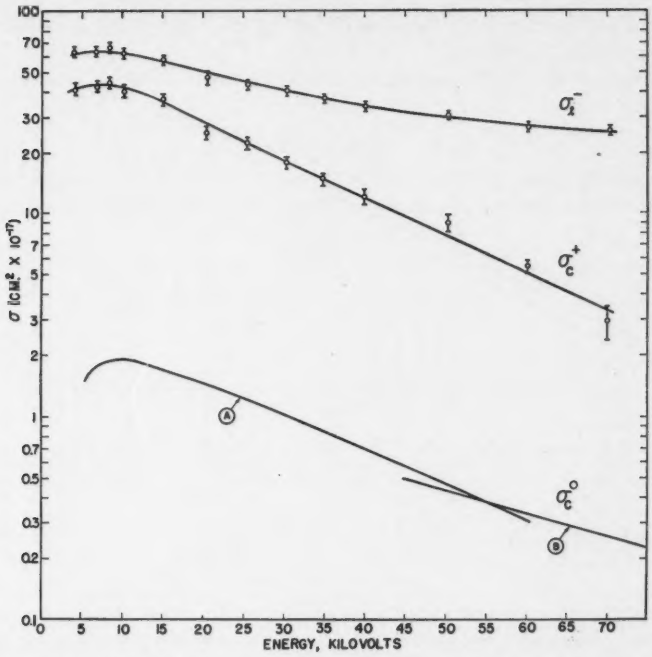

FIG. 10. The variation of σ_i^-, σ_c^0, and σ_c^+ versus energy. The σ_c^0 curve marked (A) was obtained using values of (σ_i^0/σ_c^+) from the measurements of Bartels; curve (B) was obtained using values of (σ_i^0/σ_c^+) obtained by Montague and Ribe.

Consideration of equation [1] shows that under equilibrium conditions the ratio

$$[7] \qquad (H^+/H^0)_e = \sigma_i^0/\sigma_c^+.$$

The terms of equation [4] may now be rearranged as follows:

$$\sigma_c^0 = (H^-/H^+)_e\,(\sigma_i^0/\sigma_c^+)\,\sigma_i^- = (H^-/H^+)_e\,(H^+/H^0)_e\,\sigma_i^-.$$

Now both $(H^-/H^+)_e$ and σ_i^- are known from the present work and if the ratio $(H^+/H^0)_e$ were also known over the same range of energy, one could determine σ_c^0, the electron capture cross section for neutral atoms.

The ratio $(H^+/H^0)_e$ can be obtained from the work of Bartels (2) and that of Montague (11) and Ribe (14).

Bartels measured the ratio of charged particles to neutral atoms in a beam consisting initially of homogeneous protons, after it had traversed a region containing hydrogen at sufficient pressure to produce equilibrium conditions. He assumed that this ratio was $(H^+/H^0)_e$. The results of the present experiment indicate that the ratio obtained by Bartels was actually $[(H^+ + H^-)/H^0]_e$, and from this, knowing $(H^-/H^+)_e$, it is easy to obtain $(H^+/H^0)_e$.

The values of $(H^+/H^0)_e$ or (σ_i^0/σ_c^+) obtained in this way from the work of Bartels extend over the energy range from 5 to 60 kev. At the higher energies

these values overlap with those obtained by Montague and Ribe (*loc. cit.*) and are in good agreement.

The values of σ_c^0 obtained in this way are given in the lowest curve of Fig. 10.

DISCUSSION

The errors given in Table I for σ_l^- were made up of a number of factors. The statistical fluctuations in the slope values of the curves from which σ_l^-,

TABLE I

E, kev.	$\sigma_l^- \times 10^{16}$, cm.^{2}	$\sigma_c^+ \times 10^{16}$, cm.^{2}	$(H^-/H^+)_e$,%
4.2	6.3±.4	4.2 ±.3	13.2 ± .5
6.9	6.3±.4	4.3 ±.3	20.8 ± .8
8.5	6.7±.4	4.5 ±.3	22.2 ±1.3
10.3	6.3±.4	4.1 ±.3	20.9 ± .5
15.2	5.8±.3	3.7 ±.2	14.4 ± .4
20.6	4.6±.3	2.6 ±.3	9.7 ± .6
25.6	4.3±.3	2.3 ±.2	6.5 ± .3
30.4	4.0±.2	1.8 ±.2	5.0 ± .1
35.0	3.6±.2	1.5 ±.1	3.8 ± .2
40.1	3.4±.2	1.24±.10	2.8 ± .1
50.5	3.0±.2	0.92±.09	1.48± .05
60.4	2.7±.2	0.56±.04	0.89± .03
70.3	2.5±.2	0.30±.06	0.52± .02

was calculated gave rise to an error of about 1% over the whole range of energies studied. The corresponding error in the case of σ_c^+ was greater because in this case one was dealing with the differences in the slopes of corresponding pairs of curves. This leads to an error less than 2% below 40 kev., and somewhat more than this for higher energies.

Uncertainty in the determination of the observation chamber pressure, p_0, amounted to 5% and in the ion path distance, d, the uncertainty was of the order of ±0.2 cm.

In the light of these considerations, the cumulative error in σ_l^- should not exceed 10%. The cumulative error in σ_c^+ below 40 kev. should be less than 15% and should be less than 30% for energies above 40 kev. In the case of $(H^-/H^+)_e$ the cumulative error should not exceed 7% throughout the range.

The curves of Fig. 10 show that the value of σ_l^-, the electron loss cross section for negative ions of hydrogen, varied rather less rapidly with energy than did the electron capture cross section for protons, σ_c^+. It is of interest to note that Montague (11) found that the electron loss cross section for neutral atoms of hydrogen, σ_l^0, also varied slowly with energy.

The results embodied in Fig. 11 show that in the case of the capture cross section, σ_c^+, the results obtained in the present work are in fair agreement with those obtained by Keene (7) and by Ribe (14). The values found by Goldman (3) are seen to agree with the values found at the lowest energies used.

The dotted curve marked (T) is a theoretical curve for the capture cross section, σ_c^+, obtained by Jackson and Schiff (5).

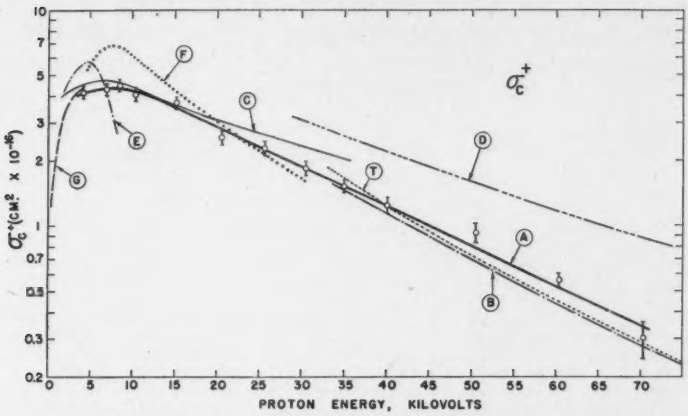

FIG. 11. A comparison of values for σ_c^+ found in the present experiment and those obtained by other workers. (*A*) the present results, (*B*) Ribe, (*C*) Keene, (*D*) Meyer (10), (*E*) Smith (15), (*F*) Bartels, (*G*) Goldman. The curve (*T*) is a theoretical one obtained by Jackson and Schiff.

Recently, Jackson* has estimated that the ratio (σ_c^0/σ_c^+) should approach a limiting value of about 0.16 for proton velocities much greater than the orbital velocity of an electron in the ground state of a hydrogen atom. The results of the present experiment show that this ratio increases from about 0.04 at 10 kev. to about 0.08 at 70 kev. One would not expect the ratio to have reached its limiting value at such relatively low energies and thus the experimental and the theoretical results are not inconsistent with one another.

ACKNOWLEDGMENTS

The author is indebted to Professor J. S. Foster, F.R.S., for his kindness in extending the facilities of the Radiation Laboratory for this work, and to Professor F. R. Terroux for his encouragement as director of the research and help in preparation of this paper. Thanks are due to Professor J. D. Jackson and to Dr. D. E. Tilley for many helpful discussions.

REFERENCES

1. ARNOT, F. L. Proc. Roy. Soc. (London), A, 158: 137. 1937.
2. BARTELS, H. Ann. Physik, 13: 373. 1932.
3. GOLDMAN, F. Ann. Physik, 10: 460. 1931.
4. HASTED, J. B. Proc. Roy. Soc. (London), A, 212: 235. 1952.
5. JACKSON, J. D. and SCHIFF, H. Phys. Rev. 89: 359. 1953.
6. KANNER, H. Phys. Rev. 84: 1211. 1951.
7. KEENE, J. P. Phil. Mag. 40: 369. 1949.
8. LAMAR, E. S., BUECHNER, W. W., and VAN DE GRAAFF, R. J. J. Appl. Phys. 12: 132. 1941.
9. LOFGREN, E. J. Rev. Sci. Instr. 22: 321. 1951.
10. MEYER, H. Ann. Physik, 30: 635. 1937.
11. MONTAGUE, J. H. Phys. Rev. 81: 1026. 1951.
12. OREAR, J., ROSENFELD, A. H., and SCHLUTER, R. A. A course given by Enrico Fermi. Revised edition. University of Chicago Press, Chicago, Ill. 1950. pp. 36, 37.

* *Private communication.*

13. PHILLIPS, J. A. Phys. Rev. 90: 532. 1953.
14. RIBE, F. L. Phys. Rev. 83: 1217. 1951.
15. SMITH, R. A. Proc. Cambridge Phil. Soc. 30: 514. 1934.
16. TUXEN, O. Z. Physik, 103: 463. 1936.
17. WHITTIER, A. C. Ph.D. Thesis, McGill University. 1952.

INDUCED INFRARED ABSORPTION IN HYDROGEN AND HYDROGEN - FOREIGN GAS MIXTURES AT PRESSURES UP TO 1500 ATMOSPHERES[1]

By D. A. Chisholm[2] and H. L. Welsh

ABSTRACT

The pressure-induced fundamental infrared absorption band of hydrogen has been investigated in the pure gas and in hydrogen–helium, hydrogen–nitrogen, and hydrogen–argon mixtures for gas pressures up to 1500 atm. and temperatures in the range 80°–376°K. At the higher densities the rate of increase of the integrated absorption coefficient with density is anomalously large; this effect is interpreted in terms of finite molecular volumes. The Q branch has been shown to consist of three components Q_P, Q_Q, and Q_R. The separation of the maxima in the low- and high-frequency components, Q_P and Q_R, depends on the perturbing gas and increases linearly with its density; the separation and relative intensities of the components are also strongly dependent on the temperature. It is proposed that this splitting of the Q branch is caused by the participation of the relative kinetic energy of the colliding molecules in the absorption process for collisions in the region of overlap forces. The Q_Q component and the S lines show no splitting and are probably produced by collisions in the region of quadrupole interaction.

INTRODUCTION

Infrared absorptions corresponding to the fundamental vibrational transition, which is forbidden by the dipole selection rules for homonuclear diatomic molecules, have been observed in compressed gaseous oxygen, nitrogen, and hydrogen (4, 18, 5). In earlier investigations these pressure-induced absorptions were studied over a range of density up to 140 Amagat units and, in the case of hydrogen, at reduced temperatures. The absorption coefficient, $\alpha(\nu)$, defined by the relation

$$I = I_0 \epsilon^{-\alpha l \rho_a}$$

where l is the path length, was found to increase linearly with the density, ρ_a, of the absorbing gas. The addition of a foreign gas causes a characteristic enhancement of the absorption of the pure gas and the absorption coefficient for the enhancement increases linearly with the density of the perturbing gas, ρ_p.* All the experimental evidence is consistent with the hypothesis that the absorption is caused by distortion of the electronic charge distribution of the molecules during close two-body collisions. Theoretical calculations of van Kranendonk and Bird (8, 9) and of Britton (2) support this interpretation.

The induced absorption in hydrogen has been the most extensively investigated and is of particular interest since several components of the fundamental and overtone bands are resolved (19). The three main maxima of the fundamen-

[1]*Manuscript received January 4, 1954.*
Contribution from the McLennan Laboratory, University of Toronto, Toronto, Ontario.

[2]*Holder of the E. F. Burton Fellowship in Physics, School of Graduate Studies, University of Toronto, 1950–1952. Present address: Bell Telephone Laboratories, Inc., Murray Hill, New Jersey, U.S.A.*

* *If the absorption coefficient is defined by the equation* $I = I_0 \epsilon^{-\alpha' l}$, α' *varies as* ρ_a^2 *for the pure gas and as* $\rho_a \rho_p$ *for the enhancement by a foreign gas. The definition used in the text simplifies the presentation. Thus,* α *varies generally as* ρ_p; *for the pure gas* $\rho_p \equiv \rho_a$.

tal band can be identified as a Q branch, and $S(0)$ and $S(1)$ lines, corresponding to the rotational transitions $\Delta J = 0$ and $\Delta J = 2$, respectively, where J is the rotational quantum number of the hydrogen molecule. A weaker line on the low-frequency side of the Q branch, which could not be interpreted in terms of a rotational transition, was a puzzling feature of the earlier results. Extension of the pressure range with pure hydrogen to 600 atm. showed that the resolution of this component improved at higher pressures (6). Further extension of the pressure range to 1500 atm. with the pure gas and with foreign gases indicated that the Q branch consists of two components (3). The component, referred to as Q_R, on the high-frequency side of the band origin as calculated for the free molecule corresponds to the main maximum; the component, Q_P, on the low-frequency side of the band origin corresponds to the weaker line that is poorly resolved at lower pressures. The frequency separation of the maxima of the two components increases with density, and is dependent on the nature of the perturbing gas and on its temperature. The intensity of the Q_P component relative to the Q_R component decreases rapidly as the temperature is lowered. No splitting of the S lines was observed with the spectral resolution used.

In the present investigation the fundamental absorption in hydrogen was studied in considerable detail for the pure gas and for mixtures with helium, nitrogen, and argon at pressures up to 1500 atm. and over a wide range of temperature. In the region of high densities the integrated absorption coefficient was found to increase with density more rapidly than expected from the simple relation observed at low densities; this effect is interpreted in terms of finite molecular volumes. Extensive data obtained on the splitting of the Q branch indicate that the origin of this phenomenon is kinetic; the relative kinetic energy of the absorbing molecule and its neighbors is altered by the absorption of the light quantum.

EXPERIMENTAL

The infrared absorption cell for high-pressure gases used in this investigation has been described (20). The light enters the cell by a pressure-tight window and, after reflection from a plane mirror of tantalum, leaves the cell by the same window. Different path lengths, up to about 4 cm., can be obtained by using annular steel spacers of different thicknesses between the window and the mirror. In the present experiments a fused quartz window, 17.5 mm. thick, and a path length of 2.1 cm. were used in most cases.

The temperature of the cell was controlled by immersing it in suitable baths contained in a metal vacuum jacket in the form of a trough. Light entered and left the cell through a tubular brass collar that was mounted on the window nut of the cell and extended through a seal in one end of the trough. This tube could be closed with a second window to prevent frosting of the cell window during low temperature experiments. For temperatures above the ambient temperature, oil was heated in a coil suspended in hot glycerine and circulated in a closed system through the vacuum jacket. For temperatures down to 200°K. an acetone bath, cooled by copper fingers filled with liquid air and projecting into the acetone, was used. Temperatures between 200°K. and 80°K. were

obtained by packing the trough with cotton waste and pouring in sufficient liquid air to give a steady temperature in the desired range. The temperature of the gas was inferred from the temperatures of the cell wall measured with a set of thermocouples attached to the body of the cell and to the window cone.

The gases were introduced into the absorption cell through the system shown schematically in Fig. 1. The gas, taken from a commercial cylinder and controlled

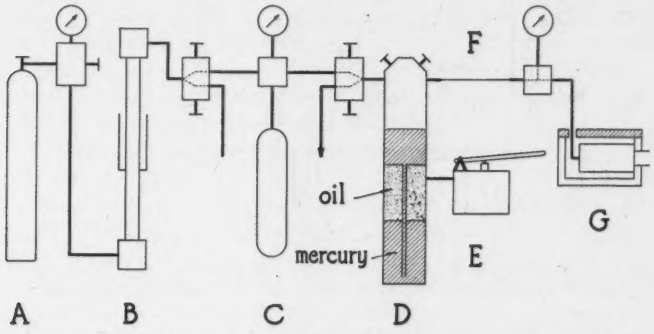

FIG. 1. Arrangement for purifying and compressing the gases. *A*, gas cylinder; *B*, purification column; *C*, storage bottle; *D*, gas compressor; *E*, oil pump; *F*, capillary tubing; *G*, absorption cell.

by a needle valve, passed slowly upwards through a purification column. The latter consisted of a 0.5 in. monel tube with detachable ends packed with bright copper turnings of graded fineness; the central section of the tube was cooled with liquid air held in a lagged vessel soldered to the tube. After leaving the purification column the gas could be stored in a stainless steel bottle at reduced temperature. The purified gas was transferred to the absorption cell through a gas compressor in which mercury formed a noncontaminating link between the gas and a hand-operated oil pump. The gas pressures were measured with Bourdon tube gauges calibrated against a dead-weight pressure balance up to a maximum of 10,000 p.s.i.; above this pressure the manufacturer's calibration had to be accepted.

The cell, tubing, and gauges were washed with Varsol, benzol, and alcohol before assembly. The high pressure sections were cleaned after assembly by filling them with liquid carbon dioxide at a pressure of at least 5000 p.s.i. This liquid penetrates all recesses of the apparatus and removes traces of oil and cleaning fluid. If the carbon dioxide is allowed to escape rapidly from the apparatus it carries with it both dissolved materials and entrained particles. Finally, the system was evacuated to a pressure of 0.1 mm. of Hg for several hours.

The infrared spectrometer used was a Perkin-Elmer instrument, model 12B, with a rock salt prism and a modified external optical system. The optical arrangement is shown in Fig. 2. The source was a 500 watt projection lamp with a planar filament, operating somewhat above its rating and stabilized with an

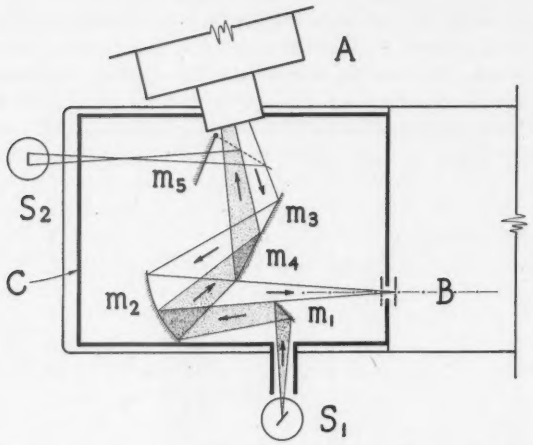

FIG. 2. Optical arrangement. A, absorption cell; B, spectrometer; C, lucite box; S_1, light source; S_2, auxiliary light source; m_1, m_3, m_4, m_5, plane mirrors; m_2, concave mirror.

electronic voltage regulator. The only significant absorption by the glass envelope of the lamp appears on the extreme low-frequency side of the hydrogen fundamental, in the same spectral region as a band due to the fused quartz window of the cell. The filaments were focused on the mirror in the cell by the mirrors m_1, m_2, and m_3, and the orientation of the cell was adjusted so that the light reflected from the mirror in the cell was focused by m_4 and m_2 on the slit of the spectrometer. With this arrangement sufficient intensity was available to utilize the ultimate resolving power of the spectrometer which is about 40 cm.$^{-1}$ in the region of the fundamental absorption of hydrogen. The optical path was completely enclosed by a lucite box which, along with the spectrometer, could be flushed continuously with dry nitrogen to remove atmospheric absorptions.

A frequency calibration curve was drawn for the spectrometer from the recorder traces of a number of bands for which frequencies are given in the literature (16, 17); as far as was possible, only frequencies determined under conditions of resolution and dispersion similar to those of the Perkin-Elmer spectrometer were used as standards. From the calibration curve a frequency scale, relating distance along the trace to frequency, was prepared. A sharp absorption band of lucite was used to position the scale on the experimental traces. In one of the several traces taken at each gas density, the mirror, m_5, was rotated into the position indicated by the dotted line in Fig. 2 to record the lucite absorption with the auxiliary source S_2.

A difficulty experienced in the experiments with gas mixtures was the reduction of the base density of hydrogen by back diffusion while a charge of foreign gas was being added; even when a large pressure difference was maintained between the supply and the cell considerable diffusion occurred in the short time the connecting valve was open. As the rate of diffusion drops rapidly with increasing pressure, this effect was important only during the addition of the first and,

perhaps, the second charge of foreign gas. However, it was found that the diffusion was negligibly small at all pressures when a length of very fine capillary tubing was inserted between the cell and the supply (Fig. 1). The addition of foreign gases in sharp pulses caused a peculiar variation in the transmission of the mixture even in spectral regions free from absorption bands. After the gas entered the cell the transmitted intensity decreased gradually, over a period of about a minute, to 25–50% of the normal value, and then returned in an exponential manner to the original level in a period sometimes as long as 45 min. When the transmission had returned to the original value it was assumed that the mixing of the gases was complete. The variation in the transmission after a pressure pulse also appeared with pure gases, the magnitude of the effect apparently increasing with the molecular weight.

Since isothermal data for mixtures of hydrogen and nitrogen in constant proportion are available in the literature (1), a test of the completeness of the mixing process and also of the effectiveness of the capillary link in preventing back diffusion of hydrogen was possible. The gases were premixed in the gas chamber of the compressor at low pressures and the mixture was compressed into the cell. This method gave absorption coefficients identical, within the experimental error, with those obtained when charges of nitrogen were added to a base charge of hydrogen; the latter method, with the precautions mentioned above, was therefore adequate.

The normal procedure in an experiment was as follows. A series of spectrometer recorder traces was taken with the cell evacuated until good reproduction indicated that the amplifier and recorder were stable. During this period the cell was brought to a steady temperature. The base charge of hydrogen was then introduced and the pressure measured with a low range gauge located at the storage bottle (Fig. 1). A series of recorder traces was then made and when the reproduction was satisfactory the first charge of the foreign gas was introduced in two or three short pulses. The transmitted intensity at a fixed wave length was recorded continuously and when the mixing of the gases appeared to be complete as judged from the end of the transient, a set of three traces of the absorption band was recorded; on one of the traces the lucite absorption was recorded for frequency calibration. An experiment consisted of observations on four to eight different gas densities. During an experiment the temperature of the gas varied by 3°K. at the most.

The average of the recorder traces for each density, after a correction for stray light had been applied, was used to calculate $\log_{10}(T_0/T)$ as a function of frequency across the band. For the pure gas T_0 is the signal transmitted by the evacuated cell and T the signal with the gas in the cell; for the enhancement by a foreign gas, T_0 refers to the cell filled with the base density of hydrogen.

The densities of the gases under the various experimental conditions were calculated from pressure–volume–temperature data available in the literature. The data were adequate for hydrogen (11, 21), helium (7), nitrogen (12, 22), and for argon above 0°C. (13). For argon at 200°K. it was necessary to obtain the density by extrapolation, since isothermal data below 0°C. appear to have been determined only up to 75 atm. (15). For mixtures of gases it was assumed

that the density of each gas could be calculated from its partial pressure. Since the relative density of the hydrogen was generally low, this procedure should be sufficiently accurate. From hydrogen–nitrogen mixture isothermals which are available (11) it was ascertained that, in this case at least, the assumption was justified.

EXPERIMENTAL RESULTS

Table I gives a summary of the experimental conditions for which one or more sets of absorption profiles were obtained. The maximum densities in most cases

TABLE I

OUTLINE OF THE EXPERIMENTS

Perturbing gas	Temperature (°K.)	Maximum density of the perturbing gas (Amagat units)
Hydrogen	90	598
	216	603
	248	514
	298	663
	333	476
	376	445
Helium	80	236
	200	803
	298	796
Nitrogen	133	660
	198	592
	298	476
Argon	200	646
	298	571
	373	515

correspond to pressures of the order of 1500 atm. The highest densities reached were usually of the order of the densities of the corresponding liquids at their normal boiling points. The liquid densities in Amagat units are: hydrogen 778, helium 692, nitrogen 647, argon 786.

The profile of the induced absorption in hydrogen is dependent on the nature of the perturbing gas, on the temperature, and, as is shown in the present investigation, on the density. A complete presentation of the experimental results would therefore require a set of graphs for each of the experimental conditions given in Table I. In Figs. 3 to 8 a selection of absorption contours is reproduced to illustrate the more salient points. Figs. 3 and 4 show the absorption in pure hydrogen and Figs. 5 to 8 the enhancement of the absorption in hydrogen by foreign gases. In these diagrams the positions of ν_0, the band origin, and the $S(0)$ and $S(1)$ lines, as calculated from the constants of the free molecule, are marked on the frequency axis. The dotted curves in Figs. 3, 5, 6, and 8 are inserted for comparison; they are the profiles calculated in each case for the highest experimental density using the specific absorption profiles obtained for the low-pressure range (5).

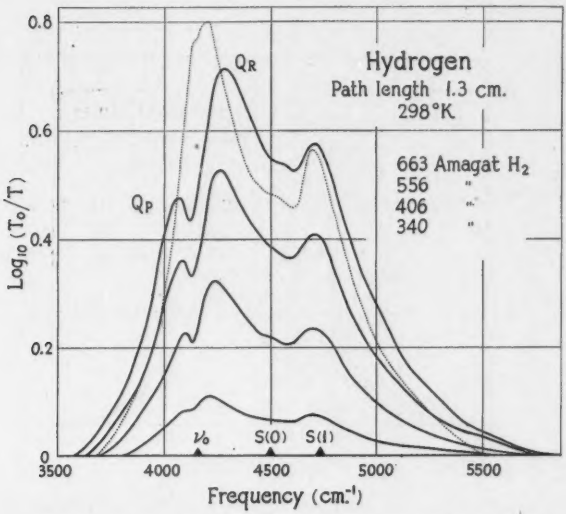

FIG. 3. The fundamental absorption in hydrogen at various gas densities. The dotted curve is the contour calculated for the density 663 Amagat using the specific absorption contour obtained in the low-pressure range.

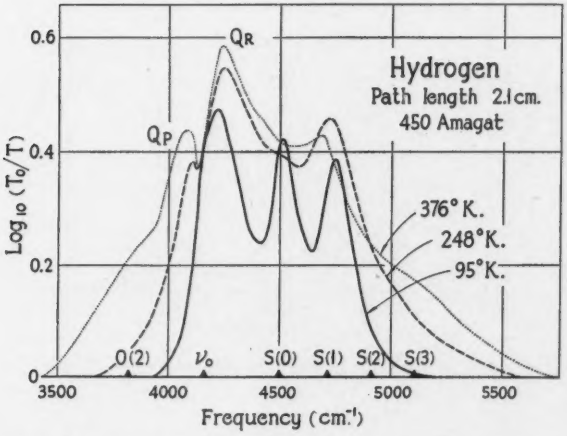

FIG. 4. The fundamental absorption in hydrogen at constant density and various temperatures.

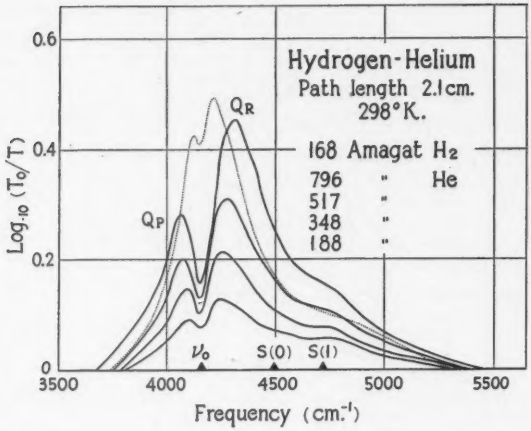

FIG. 5. The enhancement of the fundamental absorption in hydrogen by helium.

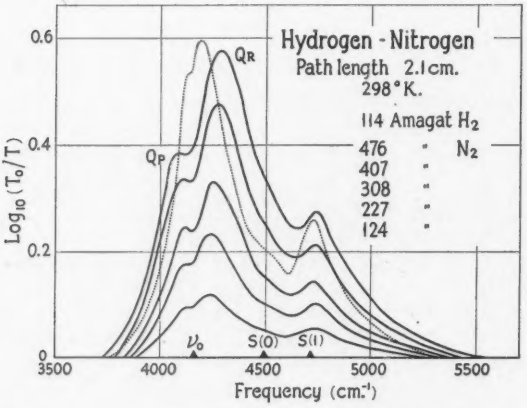

FIG. 6. The enhancement of the fundamental absorption in hydrogen by nitrogen.

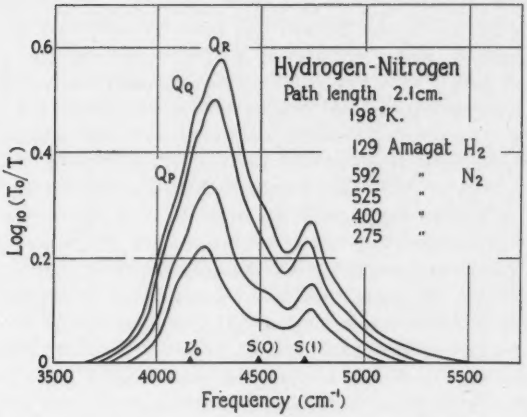

FIG. 7. The enhancement of the fundamental absorption in hydrogen by nitrogen at a reduced temperature.

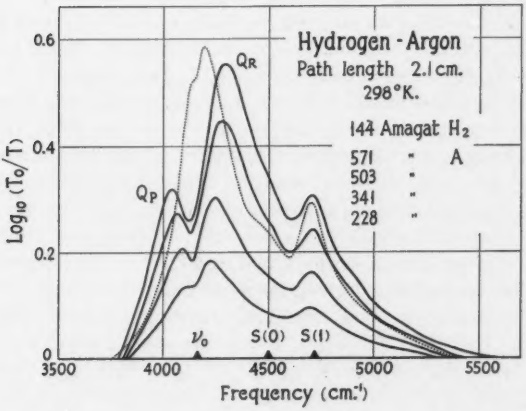

FIG. 8. The enhancement of the fundamental absorption in hydrogen by argon.

DISCUSSION

It is helpful to review some features of the induced absorption in hydrogen, already known from the experiments at lower pressures. The ratio of the intensity of the S lines to that of the Q branch is markedly different for the various perturbing gases; the ratio decreases in the order: hydrogen, nitrogen, argon, helium (Figs. 3, 5, 6, 8). The line widths, which are comparatively large at room temperature, decrease as the temperature is lowered; this fact is evident from Fig. 4 in which contours for a constant density of pure hydrogen at three widely separated temperatures are given. The reversal of the relative intensities of the $S(0)$ and $S(1)$ lines at 95°K. is a result of the lower ortho–para ratio at this temperature. With the gas at high pressure in steel vessels the equilibrium ortho–para ratio is established in a few hours and the progressive change in the ratio can be followed by recording continuously the peak intensity of the $S(0)$ line. The increase in the over-all width of the band with increasing temperature is caused not only by the increasing line width but also by the increasing population of the higher rotational levels; thus, at 376°K., the $S(2)$, $S(3)$, and $O(2)$ lines are apparent (Fig. 4). The areas under the curves of Fig. 4 show that the total intensity of absorption increases with increasing temperature.

A comparison of the contours for high gas densities with those obtained by extrapolation from the lower density data shows striking differences (Figs. 3, 5, 6, 8). The integrated intensity of absorption is clearly greater than that predicted by the simple relation found at low densities; this increased absorption at high densities is most marked for hydrogen–argon and hydrogen–nitrogen mixtures. The two components, Q_P and Q_R, of the Q branch, which are scarcely resolved at lower densities, move progressively away from the band origin towards lower and higher frequencies, respectively, as the gas density rises. The S lines, on the other hand, show no splitting and no appreciable shift in frequency. The effect of temperature on the contour of the Q branch is also very marked. As shown, for example, in Fig. 4, the magnitude of the splitting at constant density decreases and the intensity of the Q_P component falls rapidly as the temperature is lowered; in the contour for 95°K. the Q_P component is in fact no longer apparent. Although the minimum between the Q_P and Q_R components is in all cases at the band origin, ν_0, the depth of the minimum is not the same for the different mixtures; the resolution of the two components for the same instrumental conditions is best for hydrogen–helium and poorest for hydrogen–nitrogen mixtures (Figs. 3, 5, 6, 8). It was therefore surmised that there might be an additional component of the Q branch at or near ν_0. By lowering the temperature, thus decreasing the half-widths of the components and decreasing the intensity of Q_P, it was possible to resolve this additional component in hydrogen–nitrogen (Fig. 7) and hydrogen–argon mixtures. This line, which will be referred to as the Q_Q component, resembles the S lines in that its frequency is apparently independent of the gas density. Also, an examination of the profiles shows that the intensity of the Q_Q component appears to have a definite correlation with the intensities of the S lines; for example, in the hydrogen–helium mixture for which the S lines have a low relative intensity, the Q_Q line is very weak as is indicated by the deep minimum between the Q_P and Q_R components.

In the following sections the various effects found at high densities will be treated in a more quantitative manner and their interpretations will be discussed.

The Variation of the Integrated Absorption Coefficient with Density and Temperature

The quantity $\log_{10}(T_0/T)$, plotted along the ordinate axis in the curves of Figs. 3 to 8, can be transformed into an absorption coefficient, $\alpha(\nu)$ (per centimeter path length per Amagat unit of hydrogen), by multiplying by the factor $2.3/\rho_0 l$. The area under the curve can then be expressed as an integrated absorption coefficient, $\int \alpha\, d\nu$(cm.$^{-1}$/cm./Amgt.H_2). In the lower pressure experiments these absorption coefficients were found to be proportional to ρ_p, the density of the perturbing gas. At high densities the profile of the absorption becomes density dependent and $\alpha(\nu)$ is no longer proportional to ρ_p. In addition, a plot of $\int \alpha\, d\nu$ against ρ_p gave in all cases a curve indicating that the integrated absorption coefficient increases more rapidly than ρ_p. The departure from linearity was considerable for hydrogen–nitrogen and hydrogen–argon mixtures and smaller, but significant, for hydrogen–helium mixtures and pure hydrogen.

To ascertain the form of the dependence of the integrated absorption coefficient on the density, the quantity $(1/\rho_p)\int \alpha\, d\nu$ was plotted against ρ_p. For the absorption at a given temperature these graphs were found to be straight lines,

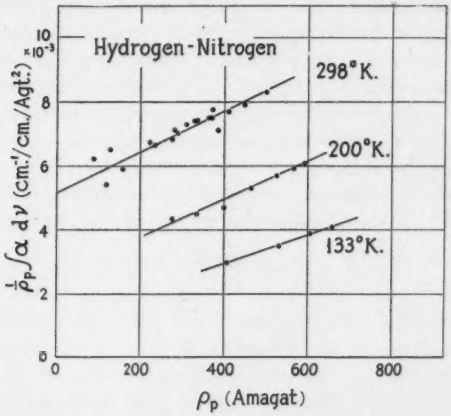

FIG. 9. The relation between the integrated absorption coefficient and the density, ρ_p, of the perturbing gas.

as shown for the enhancement by nitrogen in Fig. 9. It is therefore clear that the integrated absorption coefficient in the range studied is of the form

$$\int \alpha\, d\nu = \alpha_1 \rho_p + \alpha_2 \rho_p^{\,2}.$$

The values of the constants α_1 and α_2 determined for the various mixtures at each of the temperatures for which sufficient data were obtained are given in Table II.

TABLE II

ABSORPTION COEFFICIENTS FOR THE FUNDAMENTAL BAND OF HYDROGEN

Perturbing gas	Temperature (°K.)	Absorption coefficients		Calculated molecular diameter (Å)
		α_1 (cm.$^{-1}$/ cm./Amgt.^{2})	α_2 (cm.$^{-1}$/ cm./Amgt.^{3})	
Hydrogen	298	2.5×10^{-3}	0.2×10^{-5}	2.2
Helium	298	1.5×10^{-3}	0.1×10^{-5}	1.8
	200	1.3×10^{-3}	0.08×10^{-5}	1.8
Nitrogen	298	5.1×10^{-3}	0.6×10^{-5}	2.2
	198	2.4×10^{-3}	0.6×10^{-5}	2.8
Argon	373	5.6×10^{-3}	0.6×10^{-5}	2.1
	298	4.5×10^{-3}	0.3×10^{-5}	1.8

Since the value of α_2 is small compared with α_1, it is understandable that the departure from linearity was not detected in the experiments at lower densities. Since the terms are separated here, the values of α_1 are somewhat smaller than the values of the specific integrated absorption coefficients found in the earlier work (5). Great accuracy cannot be claimed for the values of α_1 and α_2 since they are based in most cases on limited experimental data, and since the determination of α_1 in particular requires an extrapolation to zero density.

The anomalous rise in the absorption coefficient at high densities can be interpreted in terms of the finite size of the molecules. At low densities the number of absorption-inducing collisions is proportional to $\rho_a\rho_p$; however, when the volume of the molecules themselves becomes an appreciable fraction of the space in which they are confined, the number of collisions increases more quickly than $\rho_a\rho_p$. An elementary theory of the effect, given in the Appendix, shows that the ratio of the absorption coefficients α_1 and α_2 can be expressed as

$$\frac{\alpha_2}{\alpha_1} = \frac{8\pi n_0 D^3}{9}$$

for the pure gas and as a similar expression for mixtures, where n_0 is Loschmidt's number and D the diameter of the perturbing molecule. Values of the molecular diameter calculated from the observed ratios α_1/α_2 are given in the last column of Table II; these are of the same order of magnitude as, but always somewhat smaller than, values obtained from kinetic theory calculations. It is possible that the discrepancy is caused by ternary collisions for which, on the average, the induced electric moment is smaller than for two-body collisions. The probability of ternary collisions for argon and nitrogen as perturbing molecules is greater than for hydrogen or helium since the range of the interaction forces is undoubtedly greater; thus, the difference between the calculated values of D and the kinetic theory values should be greater for argon and nitrogen, as is observed.

Finite molecular volumes have also an interesting effect on the induced absorption in the region of the first overtone of hydrogen. It has been shown

(19) that the observed lines in this region can be assigned to two transitions, a first overtone transition and a double transition in which both hydrogen molecules in the collision perform the fundamental transition simultaneously. Both bands are enhanced by the addition of foreign gases (10); however, the rate of enhancement of the double transition band is not the same as that of the overtone. It is evident that, since the double transition has its origin only in hydrogen–hydrogen collisions, its enhancement by foreign gases can occur only through a finite volume effect. Experiments now in progress indicate that this explanation is also quantitatively correct.

The integrated absorption coefficient decreases in all cases with decreasing temperature, and for hydrogen–nitrogen and hydrogen–argon mixtures the decrease is very pronounced. In a series of experiments with pure hydrogen at five different temperatures in the range 376°–216°K. the integrated absorption coefficient was found to follow the relation

$$\alpha_1 = 1.55 \times 10^{-3} + 3 \times 10^{-6}\, T$$

where T is the temperature in degrees Kelvin. At temperatures between 200°K. and 80°K. the absorption coefficient decreases more rapidly with decreasing temperature than in the higher temperature range. This effect is probably related to the changing ortho–para ratio; thus, at 80°K. the coefficient for the equilibrium mixture is only about one-half as large as the coefficient for the normal (unconverted) mixture.

A qualitative explanation of the variation of the absorption coefficient with temperature is evident from the general form of the potential curve of the colliding molecule (see Fig. 12 below). At lower temperatures the distance of closest approach is on the average greater than at high temperatures, and the interaction giving rise to the induced absorption is accordingly less. A quantitative calculation of the effect as well as the explanation of the dependence on the ortho–para ratio must await a theoretical treatment.

The Distribution of Intensity in the Q Branch

In all the cases studied the frequency separation of the Q_P and Q_R maxima, $\Delta\nu_{PR}^{\max}$, increases linearly with the density of the perturbing gas. Examples of graphs of $\Delta\nu_{PR}^{\max}$ versus density are shown in Fig. 10. The rate of increase of the separation with increasing density is characteristic of the perturbing gas, and is greatest for argon and least for helium. Extrapolation of the graphs to zero density of the perturbing gas gives values of the separation which are also characteristic of the perturbing gas; this limiting separation is greatest for helium and least for argon. The separation at zero density increases with increasing temperature, but the rate at which the splitting increases with density is not markedly dependent on the temperature. These data are summarized in Table III.

The intensity distribution in the Q_P and Q_R components bears a striking resemblance, especially at high densities, to the intensity distribution in a Bjerrum double band, that is, an infrared rotation–vibration band with unre-

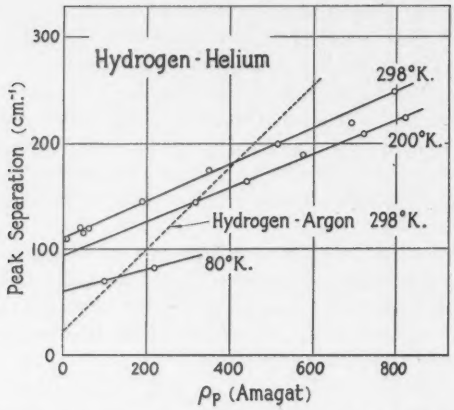

FIG. 10. Separation of the Q_P and Q_R maxima as a function of the density, ρ_p, of the perturbing gas.

TABLE III

THE SPLITTING OF THE Q BRANCH OF THE HYDROGEN FUNDAMENTAL

Perturbing gas	Temperature (°K.)	Value of $\Delta\nu_{PR}^{max}$ at low densities (cm.$^{-1}$)	Rate of change of $\Delta\nu_{PR}^{max}$ with density (cm.$^{-1}$/Amgt.)
Hydrogen	376	61	0.26
	333	50	0.26
	296	42	0.26
	248	31	0.24
	216	(4)	(0.24)
	95	The Q_P branch is not apparent as a separate maximum	
Helium	298	113	0.17
	200	95	0.16
	80	60	(0.10)
Nitrogen	298	31	0.34
Argon	373	40	0.41
	298	24	0.39
	200	(7)	(0.27)

solved rotational structure. It is easy to show that the profile of a Bjerrum double band obeys the intensity relationship

$$\ln [I_R(\nu - \nu_0)/I_P(\nu - \nu_0)] = (1/kT)[|\nu - \nu_0|]$$

where $I_R(\nu - \nu_0)$ is the intensity in the R branch at a frequency separation $(\nu - \nu_0)$ from the band origin and $I_P(\nu - \nu_0)$ is the corresponding intensity for the P branch. When the quantity $\ln [I_R(\nu - \nu_0)/I_P(\nu - \nu_0)]$, taken from the experimental profiles of the Q_P and Q_R components in induced absorption, is plotted against $|\nu - \nu_0|$, a straight line is obtained in the frequency range in

which no appreciable overlapping of the Q_P and Q_R by other components of the band occurs. The straight line passes through the origin and has reciprocal slope very nearly equal to kT. The relationship is most clearly shown for the enhancement of the absorption by helium, for which the intensities of the Q_Q and $S(0)$ lines are small. Fig. 11 shows the graph for the three high densities of

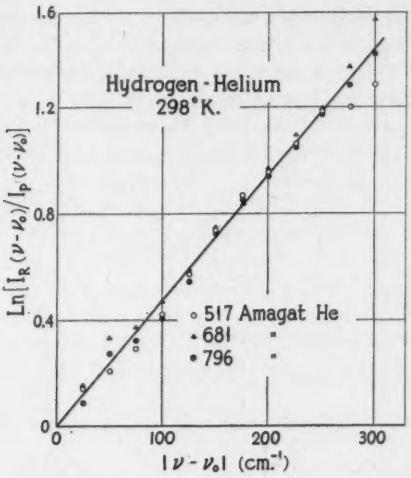

FIG. 11. An empirical relationship between $I_P(\nu - \nu_0)$ and $I_R(\nu - \nu_0)$, the intensities in the Q_P and Q_R components.

helium at room temperature. The reciprocal slope of the line drawn by a least squares analysis is 212 cm.$^{-1}$; the value of kT at 298°K. is 208 cm.$^{-1}$ Although the kT relationship and the general shape of the Q_P and Q_R components show a resemblance to a Bjerrum double band, the distribution of the intensity in the individual branches is not quite the same as in an infrared band; the extent of the Q_P and Q_R components is considerably greater than the extent of R and P branches of the infrared band with the same value of $\Delta\nu_{PR}^{\max}$.

The properties of the Q_P and Q_R components just discussed, and especially the marked changes in the band as the temperature is varied, indicate beyond reasonable doubt that the relative kinetic energy of the colliding molecules plays a part in the absorption process. Thus, in the production of the Q_R component, the absorbed photon has energy sufficient to cause the 1←0 vibrational transition in the hydrogen molecule and to impart additional relative kinetic energy to the colliding molecules; in the production of the Q_P component the energy of the absorbed photon is insufficient for the vibrational transition and the discrepancy is made up from the relative kinetic energy. In the further discussion there are essentially two effects which must be explained: (1) the splitting of the Q branch which exists at zero density and which is therefore an effect of the two-body collision producing the absorption, and (2) the linear

increase of the splitting with the density of the perturbing gas, which must be caused by the influence of neighboring molecules on the colliding pair.

The zero-density splitting of the Q branch can be explained qualitatively by considering the two colliding molecules as forming a single molecular system interacting with the light field; at the instant the absorption takes place the two molecules in close collision form an unstable "diatomic" molecule. The total relative kinetic energy of the colliding pair consists of a rotational part and a translational part, the latter equal to the relative kinetic energy along the line of centers. This division of the relative kinetic energy is clarified by the construction of effective potential curves similar to those used by Oldenberg (14) in treating molecular dissociation by rotation. If $V_0(r)$ is the potential curve for the two molecules, the effective potential curve for a noncentral collision with an angular momentum j is given by

$$V_j(r) = V_0(r) + \frac{h}{8\pi^2 c\mu r^2} j(j+1)$$

where r is the separation and μ the reduced mass of the colliding pair. Effective potential curves which are qualitatively correct for hydrogen–helium collisions are shown in Fig. 12*a*. In these curves $V_0(r)$ was calculated from the Lennard-Jones potential assumed by van Kranendonk and Bird (9) for the hydrogen–

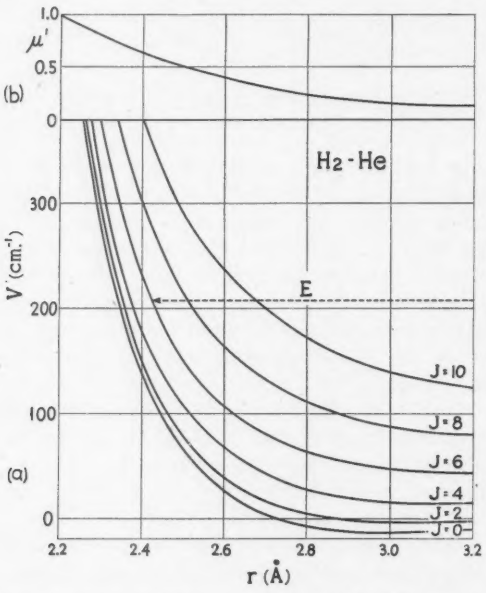

FIG. 12. (*a*) Potential curves for hydrogen–helium collisions. The effective potential curves for noncentral collisions have been drawn, for clarity, only for even values of the angular momentum, j.

(*b*) Variation of the transition moment, μ', with the intermolecular distance, r.

helium interaction. As for a stable molecule the rotational angular momentum is quantized with $j = 0, 1, 2, \ldots$; however, the rotational energy varies as $1/r^2$ and is not quantized. In Fig. 12*a* the horizontal line of constant energy represents the collision of a pair of molecules with relative kinetic energy E and angular momentum $j = 6$. The induced moment $\mu(r)$ due to the distortion of the electron distribution during the collision can be expected to decrease rapidly with increasing intermolecular distance; the part of this moment, $\mu'(r)$, which oscillates at the frequency of vibration of the hydrogen molecule gives rise to the induced absorption. The calculation of van Kranendonk and Bird shows that $\mu'(r)$ in the region of overlap forces is proportional to ϵ^{-ar}, where a is a constant depending on the particular molecules involved in the collision. The exponential form for μ', Fig. 12*b*, will therefore be assumed in the following discussion.

The participation of the relative kinetic energy in the absorption can be calculated strictly only by quantum mechanical collision theory. However, a qualitative discussion can presumably be based on dipole matrix elements of the form

$$R^{EE'} = \int \psi_E \, \mu(r) \, \psi_{E'} \, d\tau$$

where E and E' are the relative kinetic energies before and after the collision, respectively, and the ψ's are functions of r and angle variables giving the orientation of the intermolecular line, the integral being taken over the range of the variables. As the angle variables and r are not independent, the integral cannot be separated into a rotational and translational part. However, since the integral has an appreciable value only in a small range of values of r in the region of overlap forces, a separation of the variables might be assumed for a qualitative discussion. In this region the molecule behaves momentarily as a rigid rotator with a dipole moment perpendicular to the axis of rotation, and the rotational part of the matrix element would yield the selection rule $\Delta j = \pm 1$.

If it is assumed for the moment that only the rotational energy can change in the absorption the Q_P and Q_R components should have the properties of the P and R branches of an infrared rotation–vibration band. In particular, the separation of the two maxima, $\Delta\nu_{PR}^{\max}$, should follow the relationship

$$\Delta\nu_{PR}^{\max} = \sqrt{8BkT/hc} = 2.4\sqrt{BT}$$

where $B = h/8\pi c\mu r^2$. The three zero-density values of $\Delta\nu_{PR}^{\max}$ for hydrogen–helium mixtures, given in Table III, show a straight line through the origin when they are plotted against the square root of the temperature. The slope of the line corresponds to a B value of 1.7 cm.$^{-1}$ and hence to an intermolecular distance equal to 2.9 Å. From Fig. 12*a* it is seen that this value of r is approximately correct for the region of overlap forces for hydrogen and helium. It therefore appears that the participation of the rotational energy in the absorption process is very probably the reason for the splitting of the Q branch at low densities. It is, of course, evident that the individual rotational lines must be greatly broadened because of the short duration of the collision; this fact may

account for the greater extent of the Q_P and Q_R components as compared with the Bjerrum double band. Similar calculations for the intermolecular distance can be made for the other mixtures. In these cases the calculations are not so clear-cut, probably because of the distortion of the contour by the Q_Q component which is stronger than for the hydrogen–helium absorption. Nevertheless, the trend of the zero-density splitting for the various mixtures is qualitatively correct; thus, for hydrogen–argon, $\Delta\nu_{PR}^{\max}$ has a low value because of the larger intermolecular distance in the collision and the larger reduced mass.

Although the zero-density splitting seems to be explained by changes in the rotational energy alone, it is not unlikely that changes in the relative kinetic energy along the line of centers can also occur. The translational part of the matrix element, when separated out, is an overlap integral of the form

$$R^{EE'} = \int_0^\infty \psi_T \, \mu(r) \, \psi_{T'} \, dr.$$

Some properties of the integral can be deduced if the eigenfunctions are visualized as harmonic oscillator wave functions at $r_{\min}$ with the appropriate de Broglie wave lengths at large values of r. Because of the variation of μ' and the potential curve with r it is apparent that positive changes in the translational energy are more probable than negative changes; however, large changes in the translational energy are improbable.

The increased splitting of the Q branch at higher densities can also be understood as a consequence of the participation of the kinetic energy in the absorption process. Since the splitting increases linearly with the density, it is clear that ternary collisions are involved; the absorption itself is caused by a two-body collision, and any feature of the absorption which varies as the density must be caused by an interaction with a third molecule. Ternary collisions in the region of overlap forces are not significant as such collisions are comparatively rare except at very high densities. However, ternary collisions in which the third molecule is in the region of van der Waals forces are much more probable, and such collisions must give rise to the effect observed. Classically, the presence of the third molecule makes larger changes in the relative kinetic energy of the absorbing pair possible, because more kinetic energy is available and the conservation of momentum can be achieved more readily. The effect should be greatest when the perturbing molecule is large and the van der Waals forces have a long range. Thus, the splitting for argon as the foreign gas should increase more quickly with increasing density than the splitting for, say, helium; this accords with the observations.

The effect of the third molecule in the region of van der Waals forces can be incorporated by qualitative arguments into the explanation given for the zero-density splitting. The main effect is probably the removal of the restrictive selection rule $\Delta j = \pm 1$, for the two-body collision, thus making larger energy changes possible. The justification for the removal of the restriction is that the selection rule $\Delta j = \pm 1$ now applies to the whole system of three particles; classically, this means that, although the total angular momentum of the various particles of the system is preserved, it can be redistributed among the various

particles of the system. The observed intensity relationship for the Q_P and Q_R components at high densities can be interpreted by arguments similar to those used in chemical activation theory: in the production of the Q_R branch any amount of energy (within the limits imposed by selection rules) can be transformed into relative kinetic energy; however, for the Q_P branch the fractional number of collisions which can make kinetic energy E available is exp $(-E/kT)$. It is noteworthy that the linear law for the splitting persists to the highest densities reached. At very high densities more than one perturbing molecule at van der Waals distances interacts with the colliding pair. Since all of the perturbing molecules make kinetic energy available to the pair in close collision, it is probable that the splitting of the Q branch would continue to increase indefinitely as the density increases. It is proposed therefore to study this interesting phenomenon at still higher gas densities.

It is believed that the essential features of the Q branch splitting can be explained in the manner outlined without postulating possible perturbations of the vibrational frequency of the hydrogen molecule during close collisions. The splitting for hydrogen–argon mixtures at the highest densities at room temperature is nearly twelve times as great as the zero-density splitting; it is difficult to understand how argon molecules at van der Waals distances could cause a frequency perturbation so much greater than that due to the absorbing pair in close collision. It is also difficult to explain the temperature variation of the splitting in terms of perturbation of frequency; thus, for hydrogen–helium mixtures it was established that the zero-density splitting is proportional to $\sqrt{T}$ and thus disappears at the absolute zero. The explanation based on the participation of the relative kinetic energy does not suffer from these disabilities.

The experimental evidence as obtained up to the present indicates that there are two different mechanisms involved in induced infrared absorption. The S lines and the newly discovered Q_Q line have the same frequencies as the free molecule and show no splitting with increasing density. The lines of the overtone and the double transition also occur at the calculated positions and show no evidence of Q-branch splitting. One therefore concludes that one mechanism (A) is responsible for all these absorptions. On the other hand the maxima of the Q_P and Q_R components are shifted in frequency and the shift is sharply dependent on temperature and density. It must therefore be assumed that a second mechanism (B) is responsible for the production of the Q_P and Q_R components of the fundamental.

The theory of van Kranendonk and Bird throws some light on the nature of the two mechanisms. In their calculations the intensity of the induced absorption in hydrogen is separated into two parts: a part due to overlap or exchange forces, for which the induced dipole decreases exponentially with the intermolecular distance, r, and a part due to quadrupole interaction for which the induced dipole varies as $1/r^4$. The dipole moment induced by overlap forces is only slightly dependent on the relative orientation of the molecules and is ineffective in producing rotational transitions in the hydrogen molecule. The interaction in the region of overlap forces is thus primarily responsible for the production of the Q branch. The quadrupole or longer range forces produce transitions corre-

sponding to the S and O lines ($\Delta J = \pm 2$) and also a component in the Q branch ($\Delta J = 0$). It thus appears that the quadrupole interaction can be identified with the mechanism (A) postulated above and the exchange interaction with the mechanism (B). The Q_Q component corresponds to the part of the Q branch intensity produced by the quadrupole interaction. Although the theory as at present developed does not take into account the possible participation of the relative kinetic energy in the absorption process, the interpretation given above for the splitting of the Q branch seems to be qualitatively in accordance with the theory. Since the rotational energy of the colliding pair varies as $1/r^2$, changes in the rotational energy large enough to produce an observable splitting can occur only for small intermolecular distances, that is, in the region of overlap forces; thus, the S lines should show a smaller splitting than the Q branch lines. If the correlation of Q branch splitting with exchange interaction presented here is correct, it would appear that the overtone and double transition bands are almost wholly due to quadrupole interaction. An extension of the theory to explain this feature of induced absorption would be most interesting.

ACKNOWLEDGMENTS

The authors are indebted to the National Research Council of Canada for its generous and continued support of the work in high pressures at the University of Toronto.

The assistance of Dr. J. C. F. MacDonald in the earlier phases of the experimental work and of Dr. P. J. Sandiford in the calculation of the finite volume effect is gratefully acknowledged. Many discussions with Professor M. F. Crawford have been of great benefit.

APPENDIX
THE FINITE VOLUME EFFECT

The influence of finite molecular volumes on the collision frequency and thus on the coefficient of pressure-induced absorption can be estimated by a simple calculation. It is assumed that each molecule is surrounded by a sphere of volume b within which the center of any other molecule cannot penetrate. A collision which induces absorption is considered to occur whenever the center of a perturbing molecule enters the spherical shell of volume v surrounding b.

For the pure gas an average instantaneous distribution can be constructed by placing the molecules one by one into a unit volume. The probability that the nth molecule will be placed in an absorption-producing collision is $nv/(1-nb)$, and the total number of such collisions per unit volume of the gas is then

$$Z(N) = \sum_{n=0}^{n=N-1} \frac{nv}{1-nb},$$

where N is the number of molecules per unit volume. As N is very large the summation can be replaced by an integration which gives

$$Z(N) = -(v/b^2)[Nb + \ln(1 - bN)].$$

When the volume Nb is small compared to unity, a further simplification can be made. This gives

$$Z(N) = \tfrac{1}{2}vN^2(1 + \tfrac{2}{3}bN)$$

or

$$Z(\rho) = K\rho^2(1 + \tfrac{8}{9}\pi n_0 D^3\rho),$$

where ρ is the density of the gas in Amagat units, n_0 Loschmidt's number, D the diameter of the perturbing molecule, and K a constant. Thus, if the integrated absorption coefficient is of the form

$$\int \alpha\, d\nu = \alpha_1\rho + \alpha_2\rho^2,$$

the relation $(\alpha_2/\alpha_1) = (8/9)\,\pi n_0 D^3$ can be used to calculate the molecular diameter.

A similar calculation for a mixture of two gases leads to the following expression for the number of collisions:

$$Z(N_a, N_p) = \sum_{n_a=0}^{n_a=N_a-1} \frac{n_a v_a + N_p v_{ap}}{1 - N_p b_p - n_a b_a}.$$

Here the subscripts a and p designate the quantities belonging to the absorbing molecule and the foreign gas molecule, respectively. Proceeding as before one obtains

$$Z(N_p, N_a) = \tfrac{1}{2}v_a N_a^2\,[1 + \tfrac{2}{3}N_a b_a + N_p b_p] + N_p N_a v_{ap}\,[1 + N_p b_p + \tfrac{1}{2}N_a b_a].$$

The finite volume effect thus influences both the base density absorption (term in $\frac{1}{2}v_a N_a^2$) and the enhancement by the foreign gas (term in $N_p N_a v_{ap}$). However, when $N_a \ll N_p$ the first term can be considered constant and the integrated absorption coefficient of the enhancement can be written

$$\int \alpha\, d\nu = \alpha_1\rho_p + \alpha_2\rho_p^2,$$

where $\alpha_2/\alpha_1 = (4/3)\,\pi n_0 D_p^3$.

It should be noted that the condition $Nb \gg 1$ does not hold at the highest densities used in the experiments. However, the persistence of the linear relationship in Fig. 9 in the region of high densities indicates that the breakdown of the conditions is probably compensated by effects, such as overlapping of the volumes b, not taken into account in the simple theory.

REFERENCES

1. BARTLETT, J. J. Am. Chem. Soc. 49: 1935. 1927.
2. BRITTON, R. F. Ph.D. Thesis, University of Toronto. 1953.
3. CHISHOLM, D. A., MACDONALD, J. C. F., CRAWFORD, M. F., and WELSH, H. L. Phys. Rev. 88: 957. 1952.
4. CRAWFORD, M. F., WELSH, H. L., and LOCKE, J. L. Phys. Rev. 75: 1607. 1949.
5. CRAWFORD, M. F., WELSH, H. L., MACDONALD, J. C. F., and LOCKE, J. L. Phys. Rev. 80: 469. 1950.
6. DUNN, A. F. Ph.D. Thesis, University of Toronto. 1950.
7. KEESOM, W. H. Helium. Elsevier Publishing Co. Inc., Amsterdam. 1942.
8. VAN KRANENDONK, J. Dissertation, Amsterdam. 1952.
9. VAN KRANENDONK, J. and BIRD, R. Physica, 17: 953, 968. 1952.
10. MACDONALD, J. C. F. Ph.D. Thesis, University of Toronto. 1951.

11. MICHELS, A. and GOUDEKET, M. Physica, 8: 347. 1941.
12. MICHELS, A., LUNBECK, R. J., and WOLKERS, G. J. Physica, 17: 801. 1951.
13. MICHELS, A., WIJKER, HUB., and WIJKER, HK. Physica, 15: 627. 1949.
14. OLDENBERG, O. Z. Physik, 56: 563. 1929.
15. ONNES, K. and CROMMELIN, C. A. Leiden Communications No. 120. 1911.
16. PLYLER, E. K. and BENEDICT, W. S. J. Research N.B.S. 47: 202. 1951.
17. PLYLER, E. K. and PETERS, C. W. J. Research N.B.S. 45: 462. 1950.
18. WELSH, H. L., CRAWFORD, M. F., and LOCKE, J. L. Phys. Rev. 76: 580. 1949.
19. WELSH, H. L., CRAWFORD, M. F., MACDONALD, J. C. F., and CHISHOLM, D. A. Phys. Rev. 83: 1264. 1951.
20. WELSH, H. L., PASHLER, P. E., and DUNN, A. F. J. Chem. Phys. 19: 340. 1951.
21. WOOLEY, W. H., SCOTT, R. B., and BRICKWEDDE, F. G. J. Research N.B.S. 41: 379. 1948.
22. WOUTERS, W. Bydrage Tot de Kennis der Isothermen van Gasen. H. J. Paris, Amsterdam. 1946.

NOTE

A NOTE ON THE USE OF THE TITANATES AS THERMOELECTRIC TRANSDUCERS

By David G. Frood

INTRODUCTION

In theory it is always possible to convert heat efficiently into another form of energy if the entropy of the working substance (as determined in part by the parameters which characterize the other form of energy) can be made sufficiently small—or negative—on the high temperature side of a working cycle. To formalize this point, let $n_1, n_2, \ldots$ be the parameters* necessary to characterize the other energy, then the entropy at the higher absolute temperature T_1 may be written

$$[1] \qquad S(T_1, n_1, n_2, \ldots) = S_0(T_1) - s(n_1, n_2, \ldots)$$

where $S_0(T_1)$ is the "normal" thermal entropy of the working substance and $s(n_1, n_2, \ldots)$ is the contribution to the entropy due to the specific values of the parameters $n_1, n_2, \ldots$. For purposes of comparison the entropy at a lower temperature T_2 will be taken as $S(T_2) = S_0(T_2)$ so that if the change of state between these two temperatures is isentropic

$$[2] \qquad S_0(T_1) - S_0(T_2) = s(n_1, n_2, \ldots).$$

If it is assumed that $S_0 = \kappa \ln (T)$, the Carnot efficiency resulting is

$$[3] \qquad \epsilon = 1 - T_2/T_1 = 1 - \exp\{-(1/k)\, s(n_1, n_2, \ldots)\}$$

and hence $\epsilon \to 1$ as $s(n_1, n_2, \ldots) \to \infty$. Therefore if $S(T_1, n_1, n_2, \ldots)$ can be made sufficiently small, a high efficiency will result.

From these general statements, it follows that the problem of converting heat directly into electricity involves calculating the entropy of a given working substance in the presence of an electric field. For example, a dielectric showing negligible loss and characterized by a temperature dependent permittivity $\mathscr{E}_0$ has an entropy (2) in a homogeneous field E given by

$$[4] \qquad S(T, E, \mathscr{E}_0) = S_0(T) + \frac{V}{8\pi}\left(\frac{d\mathscr{E}_0}{dT}\right) E^2$$

where V is the volume of the dielectric (assumed constant with changes in temperature and field strength) and T is the absolute temperature. Other things being equal, that dielectric with the highest negative temperature gradient of permittivity would yield the highest Carnot efficiency.

It is well known that the dielectric constants of many recently discovered substances such as the titanates, niobates, tantalates, and zirconates show a strong temperature dependence; but equation [4] may not be applied directly to these solids for their permittivities also show a pronounced dependence on

*These parameters may themselves depend on the temperature.

field strength. Thus, the problem is to calculate the entropy when the dielectric constant shows a known temperature and field strength dependence and to apply the result to the solids mentioned. Unfortunately, the data necessary for a complete calculation were found for only one of these substances; namely, a 75%–25% solid solution of barium-strontium titanate. All numerical results therefore apply only to this ceramic.

THE THERMODYNAMIC PROBLEM

The steps necessary to calculate the entropy of a nonlossy dielectric showing negligible volume changes in the presence of an electric field are clearly outlined in Fröhlich (2). The extension to the case where the permittivity shows a dependence on field strength as well as temperature is straightforward.

Assuming that $\mathscr{E}(T, E) \to \mathscr{E}_0(T)$ as $E \to 0$ (where $\mathscr{E}_0(T)$ is the permittivity in "weak" fields), it follows that the displacement vector may be represented by

$$D = D(\mathscr{E}_0(T), E). \tag{5}$$

A direct calculation then yields the internal energy of a volume V of dielectric in a homogeneous field E to be

$$U(T, E, \mathscr{E}_0) = U_0(T) + \frac{V}{4\pi}\left\{\int_E E\frac{\partial D}{\partial E}dE + T\left(\frac{d\mathscr{E}_0}{dT}\right)\int_E \frac{\partial D}{\partial \mathscr{E}_0}dE\right\} \tag{6}$$

where $U_0(T)$ is the internal energy in zero field. From [6] the entropy is then

$$S(T, E, \mathscr{E}_0) = S_0(T) + \frac{V}{4\pi}\left(\frac{d\mathscr{E}_0}{dT}\right)\int_E \frac{\partial D}{\partial \mathscr{E}_0}dE \tag{7}$$

where

$$S_0(T) = \int_T \frac{1}{T}\frac{dU_0}{dT}dT$$

is the entropy in zero field strength. For the dielectrics mentioned, it is known that above the Curie temperature (T_0) there are negligible hysteresis losses and piezoelectric effects; in addition it is reasonable to assume that the losses in the frequency range of interest will be negligible. Equation [7] should thus give reliable results at temperatures above the Curie point.

It is possible to simplify [7] for the special case that D and E are related by an expression of the form

$$E = D/\mathscr{E}_0(T) + f(D) \tag{8}$$

where $f(D)$ is an arbitrary function of the displacement. It can easily be shown that [7] then reduces to

$$S(T, E, \mathscr{E}_0) = S_0(T) + \frac{V}{8\pi}\left(\frac{d\mathscr{E}_0}{dT}\right)\frac{D^2}{\mathscr{E}_0^2}. \tag{9}$$

Fortunately, the field and displacement are related in the sample to be considered by the form [8] so it is possible to calculate the heat input and Carnot efficiency for this solid fairly easily.

RESULTS FOR A 75% – 25% SOLID SOLUTION OF BARIUM-STRONTIUM TITANATE

Roberts (3) has measured the temperature and field dependence of dielectric constant for a 75%–25% solid solution of barium-strontium titanate. His results indicate that above the Curie temperature ($T_0 = 298°K.$) the permittivity in "weak" fields follows the law

$$\mathscr{E}_0 = \frac{1}{\beta(T - T_0)} \tag{10}$$

where $\beta \simeq 1.35 \times 10^{-5}/°C$. Furthermore, the displacement and field are related by

$$E = D/\mathscr{E}_0(T) + \eta D^3 \tag{11}$$

where: $\eta \simeq 5.4 \times 10^{-15}$ cm.^{2}/(statt-volt)^2. The only real root of [11] is

$$D = \left(\frac{1}{\eta}\sqrt{\left(\frac{E}{2}\right)^2 + \frac{1}{27\eta\mathscr{E}_0{}^3}} + \frac{E}{2\eta}\right)^{1/3} - \left(\frac{1}{\eta}\sqrt{\left(\frac{E}{2}\right)^2 + \frac{1}{27\eta\mathscr{E}_0{}^3}} - \frac{E}{2\eta}\right)^{1/3} \tag{12}$$

which may be expanded in series to give

$$D = \mathscr{E}_0 E \sum_{k=0}^{\infty} a_k \cdot \frac{\zeta^{2k}}{(1 + \zeta^2)^{k+1/3}} \tag{13}$$

where $\zeta^2 = \frac{1}{4}E^2(27\eta\mathscr{E}_0{}^3)$ and

$$a_k = \frac{2 \cdot 5 \cdot 8 \ldots (6k - 1)}{3^{2k}(2k + 1)!\,(1 - 2\delta_{k,0})}.$$

Although [13] converges for all $\zeta^2 < \infty$ this process is not rapid for $\zeta^2 \gg 1$. A second expansion of [12], given by

$$D = \left(\frac{E}{\eta}\right)^{1/3}\left\{1 - \frac{1}{(4\zeta^2)^{1/3}} - \frac{1}{4\zeta^2} + \ldots\right\}, \tag{14}$$

is therefore needed for the case of "high" field strengths; i.e., for

$$\zeta^2 = \tfrac{1}{4}E^2(27\eta\mathscr{E}_0{}^3) \gg 1.$$

The transducer (which is merely a simple condenser operating between the temperatures T_1 and T_2—with $T_1 > T_2 \geqslant T_0$) has a Carnot cycle like that shown in Fig. 1. The isothermals AB and CD are two of the family of curves given by [11], whilst BC and DA are the adiabatics. The heat drawn in at the higher temperature by reducing the field from E_A to E_B isothermally is readily calculated from equation [9] to be

$$Q_1 = T_1[S(T_1, E_B, \mathscr{E}_0) - S(T_1, E_A, \mathscr{E}_0)];$$

therefore

$$Q_1 = \frac{VT_1}{8\pi}\left|\left(\frac{d\mathscr{E}_0}{dT}\right)_{T_1}\right| \cdot \frac{D_A{}^2 - D_B{}^2}{\mathscr{E}_0{}^2(T_1)} \tag{15}$$

where D_A and D_B are the displacements corresponding to the points A and B and are calculated from [13] or [14]. The total output of electrical energy from a complete cycle is then

$$W = \frac{V}{4\pi}\oint E\,dD = Q_1\epsilon \tag{16}$$

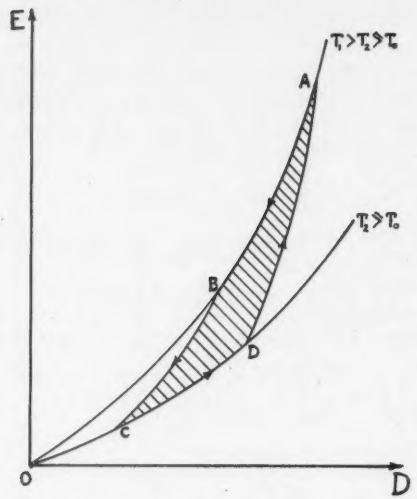

FIG. 1.

where ϵ is the Carnot efficiency. If the point B is considered to be still in the region of "high" field strength, the adiabatic cooling possible by "switching off" this field to some negligibly small value is seen from [9] and [14] to lead to an efficiency

$$[17] \qquad \epsilon = 1 - \exp\left\{\frac{-\beta}{8\pi\rho c_0}\left(\frac{E}{\eta}\right)^{2/3}\right\}$$

where ρ is the density and c_0 the specific heat in zero field strength.* Taking $\rho \simeq 2$ gm./cm.^{3}, $c_0 \simeq 0.10$ cal./gm., equation [17] predicts for pre-breakdown fields (10^5 volts/cm.) an efficiency of only about 1%.

Had the field dependence of the dielectric constant been zero; i.e., $\eta = 0$ (all other properties being the same), [4] predicts for the efficiency

$$[18] \qquad \epsilon = 1 - \exp\left\{\frac{-\beta}{8\pi\rho c_0}(\mathscr{E}_0^2 E^2)\right\}.$$

Starting from a temperature $T_1 = 321.5$°K. ($\mathscr{E}_0 \simeq 3100$) and the same field strength as before, [18] predicts an efficiency of about 7% or a cooling to about the Curie temperature. Clearly this efficiency is the maximum obtainable for the field strength used if the permittivity is assumed to be temperature dependent alone.

CONCLUSIONS

Rough calculations on a 75%–25% solid solution of barium-strontium titanate exclude its use as a reasonable thermoelectric transducer. Similar conclusions would probably hold for the other high $\mathscr{E}$ materials mentioned. In

The known small anomaly in specific heat (1) near the Curie temperature has of course been neglected here since it is a second order effect.

view of these facts it is, therefore, very difficult to take a positive point of view to the proposals mentioned. It seems sufficient to say that, if the field strength dependence of the dielectric constant could be removed for some high $\mathscr{E}$, high $|d\mathscr{E}/dT|$ materials (the other significant properties being unchanged —or favorably changed in the sense indicated by [18]), a transducer with an efficiency comparable to that of a steam engine could be developed.

ACKNOWLEDGMENTS

The permission of the National Research Council to publish this paper is gratefully acknowledged. The author also wishes to thank Mr. W. F. Campbell and Dr. D. K. C. MacDonald for helpful criticisms and suggestions and Dr. D. C. MacPhail who proposed the basic problem.

1. BLATTNER, H. and MERZ, W. Helv. Phys. Acta, 20: 210. 1948.
2. FRÖHLICH, H. Theory of dielectrics. Oxford University Press, London. 1949. pp. 9–12.
3. ROBERTS, S. Phys. Rev. 71: 890. 1947.

RECEIVED SEPTEMBER 28, 1953.
DEFENCE RESEARCH TELECOMMUNICATIONS ESTABLISHMENT,
DEFENCE RESEARCH BOARD,
OTTAWA, ONT.

CANADIAN JOURNAL OF PHYSICS

Notes to Contributors

Manuscripts

(i) ***General.*** Manuscripts should be typewritten, double spaced, on paper 8½×11 in. **The original and one copy are to be submitted.** Tables (each typed on a separate sheet) and captions for the figures should be placed at the end of the manuscript. Every sheet of the manuscript should be numbered.

Style, arrangement, spelling, and abbreviations should conform to the usage of this journal. Names of all simple compounds, rather than their formulas, should be used in the text. Greek letters or unusual signs should be written plainly or explained by marginal notes. Superscripts and subscripts must be legible and carefully placed.

Manuscripts should be carefully checked before they are submitted; authors will be charged for changes made in the proof that are considered excessive.

(ii) ***Abstract.*** An abstract of not more than about 200 words, indicating the scope of the work and the principal findings, is required, except in Notes.

(iii) ***References.*** References should be listed **alphabetically by authors' names,** numbered, and typed after the text. The form of the citations should be that used in this journal; in references to papers in periodicals, titles should not be given and only initial page numbers are required. All citations should be checked with the original articles and each one referred to in the text by the key number.

(iv) ***Tables.*** Tables should be numbered in roman numerals and each table referred to in the text. Titles should always be given but should be brief; column headings should be brief and descriptive matter in the tables confined to a minimum. Numerous small tables should be avoided.

Illustrations

(i) ***General.*** All figures (including each figure of the plates) should be numbered consecutively from 1 up, in arabic numerals, and each figure referred to in the text. The author's name, title of the paper, and figure number should be written in the lower left corner of the sheets on which the illustrations appear. Captions should not be written on the illustrations (see Manuscript (i)).

(ii) ***Line Drawings.*** Drawings should be carefully made with India ink on white drawing paper, blue tracing linen, or co-ordinate paper ruled in blue only; any co-ordinate lines that are to appear in the reproduction should be ruled in black ink. Paper ruled in green, yellow, or red should not be used unless it is desired to have all the co-ordinate lines show. All lines should be of sufficient thickness to reproduce well. Decimal points, periods, and stippled dots should be solid black circles large enough to be reduced if necessary. Letters and numerals should be neatly made, preferably with a stencil (**do NOT use typewriting**), and be of such size that the smallest lettering will be not less than 1 mm. high when reproduced in a cut 3 in. wide.

Many drawings are made too large; originals should not be more than 2 or 3 times the size of the desired reproduction. In large drawings or groups of drawings the ratio of height to width should conform to that of a journal page but the height should be adjusted to make allowance for the caption.

The original drawings and one set of clear copies (e.g. small photographs) are to be submitted.

(iii) ***Photographs.*** Prints should be made on glossy paper, with strong contrasts. They should be trimmed so that essential features only are shown and mounted carefully, with rubber cement, on white cardboard.

As many photographs as possible should be mounted together (with a **very** small space between each photo) to reduce the number of cuts required. Full use of the space available should be made and the ratio of height to width should correspond to that of a journal page; however, allowance must be made for the captions. Photographs or groups of photographs should not be more than 2 or 3 times the size of the desired reproduction.

Photographs are to be submitted in duplicate; if they are to be reproduced in groups one set should be mounted, the duplicate set unmounted.

Reprints

A total of 50 reprints of each paper, without covers, are supplied free. Additional reprints, with or without covers, may be purchased.

Charges for reprints are based on the number of printed pages, which may be calculated approximately by multiplying by 0.6 the number of manuscript pages (double-spaced typewritten sheets, 8½ × 11 in.) and making allowance for illustrations (not inserts). The cost per page is given on the reprint requisition which accompanies the galley.

Any reprints required in addition to those requested on the author's reprint requisition form must be ordered officially as soon as the paper has been accepted for publication.

Contents

Page

An Ionization Manometer and Control Unit for Extremely Low Pressures—*P. A. Redhead and L. R. McNarry* - - - - - - 267

Fast Negative Hydrogen Ions—*A. Charles Whittier* - - - - - - 275

Induced Infrared Absorption in Hydrogen and Hydrogen – Foreign Gas Mixtures at Pressures up to 1500 Atmospheres—*D. A. Chisholm and H. L. Welsh* - - - - - - - - - - - - - - 291

A Note on the Use of the Titanates as Thermoelectric Transducers—*David G. Frood* - - - - - - - - - - - - - - - - - - 313

Printed in Canada *by* University of Toronto Press